Montana Bureau of Mines and Geology

PROCEEDINGS

Original artwork by Bulbul Majumder, MBMG.

Montana Mining and Mineral Symposium 2021

September 9–September 11, 2021

Montana Bureau of Mines and Geology

Special Publication 123

TABLE OF CONTENTS

Deep Sediment-Hosted Porphyry Copper Deposits with Critical Mineral Potential and the Geochemical Relationship of Orbicular Actinolite Alteration to District Zoning and Oxidation by Carbonate Dissolution CO_2 Release

George H. Brimhall

Clementine Exploration LLC, Wise River MT and

Earth and Planetary Science, Emeritus Professor of Geology

University of California, Berkeley

Abstract

Deep syntectonic sediment-hosted porphyry copper deposits occurring within Sevier fold and thrust belt anticlines in Montana are structurally controlled and hydrodynamically confined. Hence, these porphyry systems can exhibit limited upward indicators of early high-temperature alteration, and little evidence for a clear porphyry to epithermal environment of mineralization. These characteristics are unlike similar porphyry mineral deposits found in plutonic and volcanic wall rocks in the Chilean Andes. These differences therefore require a modification of the porphyry copper model. A revised model for porphyry copper deposits is presented here for systems that form above the frontal Sevier thrust and interact with thick Paleozoic through early Triassic sedimentary platform sequences, often within anticlinal domes referred to here as "apex" exploration targets. Besides recognizing structural controls, the passive Atlantic-style margin platform sedimentary sequences in our model are considered as having great importance far surpassing the subordinate role ascribed to mere wall rocks in relation to later short-lived but ore-forming magmatic-hydrothermal systems. Instead, platform sediments with great lateral consistency and predictability are integral parts of a composite crustal-scale metallogenic system with depositional, erosional, and exposure features formed from Cambrian to Triassic time.

Varied well-known geological attributes of the sedimentary sequences affect and enhance ore deposition. Attributes of the evolved sedimentary system are incorporated into the porphyry copper ore genesis model as interdisciplinary knowledge, including sequence stratigraphy, global unconformities, paleo-karst, and basin evolution and redox cycling. Unprecedented opportunities emerge that support value-added metallic resources that expand the copper base to include rare earth elements (REEs) in Permian age phosphate deposits, and potential for Leadville, Colorado-style unconformity-related paleo-karst high-grade Cu-Ag vein and mantos replacement ore bodies. The acronym for the new modified model is termed the Deep Apex Sediment-Hosted Enhanced Resource, or the DASHER porphyry copper deposit (PCD) model. Putting REEs into a copper perspective shows that the *in situ* value of REEs in the Retort member of the Phosphoria formation in southwest Montana contains from about 0.3 to 1.25% copper value equivalent and the P_2O_5 phosphate contains about 1 to 1.5% copper value equivalent, indicating that REEs alone in the Phosphoria may locally double the value of contained base metals. Superimposed on these strata-bound mineral resources are magmatic-hydrothermal processes typical of traditional PCDs. The zoning pattern includes distal orbicular actinolite alteration, which was first recognized at Bingham Canyon, Utah and related to early high-temperature Potassic alteration. At the Clementine prospect, which is the type example of the DASHER PCD model, this actinolite orb zone occurs as a large 3 by 5 km ring pattern that dips outward, implying a high-level position. This Sevier-age (70.1 Ma) alteration ring surrounds and is coaxially aligned with the axial plane of a doubly plunging anticlinal dome. Along the apex of the anticline is a system of mineralized breccia vein gossans containing up to 3,700 ppm As, 2,300 ppm Sb, and 3,000 ppm Ba, with an exposed strike length of 1.5 km and a large elliptical zone containing barren breccias with two granitic plutons occurring on the east side. Since the sedimentary sequence at Clementine has 700 m of reactive Madison limestone and 180 m of carbonaceous Jefferson dolomite at depth, the full range of magma-derived metals is expressed in addition to the syngenetic REEs in the Phosphoria formation. In order to prove that the actinolite orbicular zone is in fact an integral part of the PCD system, a new chemical thermodynamic phase diagram is presented here in log fugacity CO_2/CH_4 vs log fugacity H_2S coordinates, showing the orbs in relation to

well-known mineral assemblages in the PCDs in relation to the sedimentary source rocks of basinal brines and hydrocarbons. Using sulfide, oxide, and alteration silicate mineral assemblages as guideposts, porphyry copper mineral assemblages form a definitive trend line along which the actinolite orbs plot, representing the outer and upper interaction zones with porous wall rock sedimentary formation pore fluids where actinolite forms within orbs by diffusion at the edges of advection with CH_4-dominated reduced fluids. This co-linearity of the orbs with the porphyry copper trend line and their location at the reduced end where granitic wall rock mineral buffers and sedimentary fluid sources converge proves the genetic linkage with early high-temperature porphyry copper mineralization, removing any doubt that mapped actinolite orb rings are indicative of potentially important porphyry copper mineralization. Furthermore, closed ring patterns coaxial with high Sb, As, and Ba veins serve as a powerful targeting tool. The phase diagram explains why carbonate-bearing sedimentary wall rocks exert a far stronger hydrolysis effect on hydrothermal fluids than volcanic and plutonic wall rocks. Acid attack of thick sections of carbonates produces CO_2 gas, which rapidly elevates the CO_2/CH_4 ratio and drives the fluid composition towards a higher oxidation state along the porphyry copper trend line from the chalcopyrite–pyrrhotite boundary up into the bornite and chalcocite fields along and past the edge of the granitic wall rock and actinolite buffer boundaries. Compared to volcanic-hosted PCDs, carbonate dissolution also broadens the array of minerals precipitated so that a fuller expression of the overall suite of metals being transported from the parental magma is made possible, including W, As, Sb, Ga, Te, Bi and Se. Furthermore, given the passive Atlantic style tectonic margin and related sequence stratigraphy of the Paleozoic age sediments, it is likely that four well-known unconformities may control paleo-karst along which high-grade Leadville, Colorado-style mantos and vein systems developed. As deep porphyry enhanced resource targets high-grade hypogene mantos may serve, along with the REEs and P_2O_5 in the Phosphoria as the critical value-added economic boost to copper grade previously offered by supergene enrichment, but without the need to strip and relocate the inevitable voluminous leached cap waste rocks. Taken as a whole, the DASHER PCD targets offer substantial new opportunities for discovery of domestic supply-chain-constrained critical and basic minerals. Given the range of traditional PCD mineralization, the enhanced resource character of the DASHER targets could support an unusual flexibility in utilization of underground space during the mine life cycle that minimizes the environmental footprint on the surface through back-filling of space by development and processing wastes. Over time, acceptance of the DASHER PCD model and innovations in underground mining might help soften if not transform the current negative attitudes about mining as a purely extractive industry and replace it with understanding and appreciation of ore deposits as the primary origination point for a sustainable energy future. Earning a social license for domestic mining starts with aspiring to transform social attitudes through making authentic progress in reimagining what the mine life cycle means.

Introduction

Knowledge of porphyry copper deposit genesis used in exploration today is based upon research in mines where the porphyritic parental intrusions encountered volcanic or plutonic wall rocks considered largely as a passive backdrop for mineralization (Lowell and Guilbert, 1970; Gustafson and Hunt, 1975; Seedorf and others, 2013; Sillitoe, 2010). However, exploration in Montana, with the expanse of the Sevier-age fold and thrust belt, requires consideration of the role of sediments in a new light. Therefore, this paper addresses six challenges in porphyry copper (PCD) exploration in terranes with abundant sedimentary rock formations: First, describing the regional geology of the Sevier-age fold and thrust belt of Montana in terms useful for exploration for deep sediment-hosted porphyry copper deposits. Second, updating the PCD model to incorporate structural and stratigraphic controls using the Clementine prospect as the type system. Third, devising new thermodynamic phase equilibria in the CO_2/CH_4-H_2S framework appropriate to explain fluid interaction with sedimentary as well as igneous mineral assemblages. Fourth, using these equilibria to rigorously prove and explain the association of orbicular actinolite alteration with early high-temperature porphyry copper zonation and Potassic alteration. Fifth, evaluating the opportunities for value-added metallic resources contained in the sediments including phosphate and rare earth elements (REEs), and finally, describing the potential for unconformity-related, paleo-karst high-grade Cu-Ag vein and mantos replacement ore bodies.

The common dissociation of magmatic-hydrothermal and stratiform ore deposits reflects in part a lack of a comparative geochemical framework, which depicts the composition of ore-forming fluids spanning both magmatic sources and hydrocarbon, brine, and meta-sedimentary fluids from which possible interrelationships might be discerned or discounted. Thus, without understanding how magma, sedimentary wall rocks, and sediment-derived fluids may comingle under certain geological circumstances, exploration for sediment-hosted PC deposits in the Sevier fold and thrust belt will remain poorly informed by geoscience and opportunities can be overlooked. This dichotomy is in part a hard-rock versus soft-rock division in geoscience education that persists in professional specialization within industrial sectors of materials (metals and mining) versus energy (oil and gas), thus largely divorcing ore genesis from petroleum geology, and even splitting science from engineering. However, today, clean sustainable green energy by decarbonization and electrification of the U.S. economy requires transformative solutions not limited by technical legacies imposed by historic scientific and engineering subdivisions. Newly mined critical and basic minerals, especially copper, are needed to support production of electric vehicles, semiconductor electronics, magnets, and lithium storage at an unprecedented level of demand. Petroleum geologists and geophysicists displaced as the shift towards carbon-zero energy advances have expertise and command of massive datasets synthesized by the American Association of Petroleum Geologists (AAPG) globally through corporate sharing of information and State and Federal partnerships, which are rare in mining. The wealth of soft-rock knowledge and expertise could synergize with the economic geology by helping to create unprecedented multidisciplinary exploration models of merit. The development of a domestic supply chain starts with raw materials produced sustainably with a transparency demanded by the necessity of earning a social license for mining through deep mine development with a minimal environmental footprint. We start here then presenting porphyry copper deposit exploration in Montana using an AAPG tectonic map based on a tectonically classified stratigraphic framework contained in the AAPG Correlation of Stratigraphic Units (COSUNA), widely used in petroleum exploration.

Regional Geology and Broad Controls on Mineralization

The AAPG tectonic map (fig. 1, next page) covers parts of Montana, Utah, and Colorado. In blue are platform sediments that formed on an expansive Atlantic-style passive tectonic margin (Dickinson, 1981). The sediments therefore correlate throughout the western U.S. and consist of recurrent depositional cyclic sequences of sandstone, shale, and limestone. The color patterns are deliberately vivid so as to highlight certain tectonic-stratigraphic units of central importance. Notice also that basement rocks below the platform sequence are shown in red, contrasting sharply with the use of red in economic geology to demark igneous rocks. Here such magmatic systems are shown in green. Larry Sloss worked throughout the western and eastern U.S. defining cratonic, onlapping mega sedimentary sequences that were named after the Indian tribes indigenous near where a sequence was best observed and defined by regional unconformities (Sloss and Laird, 1947; Sloss and Moritiz, 1951; Sloss, 1963. The cratonic sequence stratigraphy defined five intercontinental unconformities from oldest to youngest: the Sauk, Tippecanoe, Kaskaskia, Absoroka, and Zuni (Sloss and Laird, 1947; Sloss and Moritz, 1951; Sloss, 1967) shown in figure 1A. These unconformities result largely from global episodes of marine transgression and regression. Long intervals of non-deposition and erosion, shown as squiggly lines, are unconformities on which paleo-karst may have developed. The importance of recognizing these unconformities is historic and deserves acknowledgement here, where we apply this knowledge to exploration for metallic minerals. Recursive graphical elements such as unconformities are included in the following figures to develop the narrative linking interdisciplinary processes. The field of sequence stratigraphy was started by Larry Sloss, who worked at the Montana Bureau of Mines and Geology and Montana Tech for 7 years in the 1940s. Later, one of Sloss's graduate students at Northwestern University, Peter Vail, started the field of seismic stratigraphy (Vail and others, 1977a), from which global sea levels and eustatic curves over time have emerged (Vail and others, 1977b) while working for Exxon (Dott, 1992, 2014),

While the porphyry and vein ore deposits at Butte (shown as a red dot in fig. 1) are related to porphyritic magmas that intruded plutonic Butte Granite wall rocks shown in green, sediment-hosted deposits like Bingham Canyon formed where the intrusions invaded thick sedimentary sequences (represented here in light blue on fig. 1). At Bingham, the Mississippian-Missourian age Yampa and Highland limestones, which are in the middle

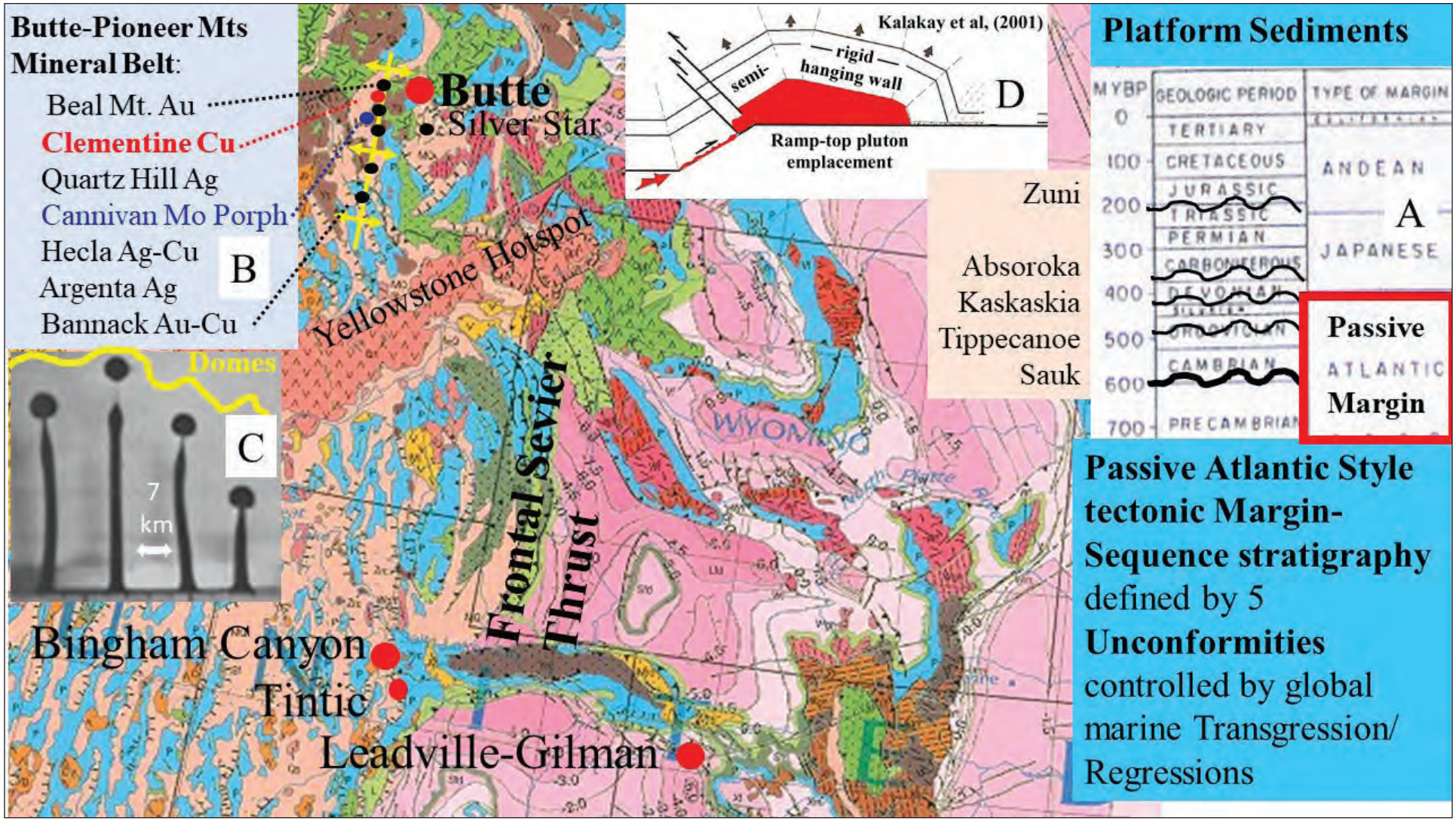

Figure 1. AAPG tectonic map based on COSUNA sections. North–south-trending blue patterns in lower left are due to east–west Basin and Range extension along listric faults. (A) Plate tectonic margin styles through time from Dickinson (1981) with intercontinental unconformities shown as squiggly black lines (Sloss and Moritiz, 1951; Sloss 1963) are the (C) 7 km average spacing between magma plumes. (B) The Butte–Pioneer Mountain mineral belt of Brimhall and Marsh (2017) and the position of the Clementine prospect in relation to known mining districts. (C) Rayleigh–Taylor gravitational instabilities forming magmatic plumes modeled by Bruce Marsh with an equal spacing of about 7 km. Each of the ore deposits in B form at structural domes, shown in yellow lines along the regional north–south-trending anticlinorium in B. (D) The idealized laccolith formed in the hanging wall of the frontal Sevier Thrust (Kalakay and others, 2001) where we assert that magmatic plumes ascended up the fault ramps.

part of the Oquirrh Group (locally called the Bingham Mine Group), were altered to *proximal* mineralized skarn up to a maximum distance of 400 m from the intrusion (Atkinson and Einaudi, 1978, fig. 7B). The pre-Tertiary structures interpreted by Atkinson and Einaudi (1978) to be bedding plane faults at the base of the Highland Boy limestone played an important role in determining the geometry of orebodies in the sedimentary rocks of the contact aureole of the Bingham Stock and in causing high concentration of sulfides. Alternatively, inspection of AAPG CONSUNA Charts Great Basin (GB; Oquirrh Mountains Column 26 and Central Wasatch Column 27 by Hintze and others, 1985) shows that the base of the Bingham Mine Group may, instead of being a bedding plane fault, be a regional unconformity that controlled fluid migration. An indisputable example of unconformities playing a role in mineralization are high-grade Cu-Ag veins, and *distal* carbonate replacement manto ores developed in aerially widespread super-unconformity paleo-karst carbonate aquifers as in the Leadville and Gilman districts of the Central Colorado mineral belt southeast of Bingham (Beaty and others, 1990; Sando, 1988). The top of the Leadville Limestone of Mississippian age is a super-unconformity shown in the AAPG CONSUNA Charts Central and Southern Rockies (CSR) (Kent and others, 1988; Piceance Basin Column 17 by Al Sanborn) on which high-grade mineralization developed in paleo-karst (De Voto, 1988) serving as permeable pathways that cross stratigraphy. Unlike igneous-hosted PCDs, sediment-hosted porphyry systems share a vast lateral continuity of the stratigraphy and regional unconformities, which implies that Cu-Ag vein and mantos systems developed in paleo-karst in Colorado can be expected in Montana.

In southwest Montana (shown in the northwest corner of fig. 1), the same Mississippian super-unconformity controlling mantos carbonate replacement ore deposition at Leadville, Colorado occurs and is shown in AAPG CONSUNA Charts Northern Rocky/Williston Basin (NRW; Ballard and others, 1983; Butte, Bozeman, SW Montana Column 9 by Susan Vuke). In figure 1B, a linear belt of geochemically varied intrusion-related (Au, Ag, Cu, W, and Mo) historic mining districts occurs and is listed as shown with Beal Mountain gold on the north to Bannack on the south. Brimhall and Marsh (2017) termed this the Butte Pioneer Mountains mineral belt. The regular spacing of these deposits is about 7 km through the Pioneer Mountains. Most of these districts are localized within dome structures and occur along a single north–south-trending regional anticlinorium of the frontal (easternmost) anticline of the Cordilleran fold and thrust belt of Sevier (Late Cretaceous) age, shown in yellow (Zen, 1988). We proposed a mechanism that explains the regular spacing of mining districts, a theme that has been fundamental in focusing our fieldwork leading to geological discoveries at Clementine (shown in red, fig. 1). From aerially extensive buoyant ribbon-like layers of magma presumably existing at depth along thrust fault flats, our calculations show diapiric ascent occurring at a regular spacing determined by Rayleigh–Taylor gravitational fluid (magmatic) instabilities (fig. 1C). Using our regional exploration model with both its regional structural and magma self-organizational aspects, Brimhall recognized a gap between the Beal Mountain and Quartz Hill Districts. Consequently, he focused fieldwork on the former Divide District, which had no prior history of metal production but occurs at a suggestive spacing with an associated anticlinal fold. Through digital mapping within a nappe window into the Lewis overthrust, Clementine Exploration LLC discovered a mineralized syntectonic frontal thrust fault-bend anticline consistent with the idealized east–west cross-section published by Kalakay and others (2001; fig. 1D; based upon earlier work Schmidt and others, 1990) as part of the Boulder Batholith mapping project of the U.S. Geological Survey. This model of syncompressional laccolith formation has been adopted for the Clementine prospect (shown in fig. 1B) within a linear belt of mining districts exposed at different erosion levels. On the north end, the surface at the Beal Mountain gold deposit is in Cretaceous age sediments of the Black Leaf Formation at a relatively high stratigraphic level. Clementine surface exposures extend from Black Leaf down to Mississippian age Madison. Quartz Hill through Bannack occur within older sedimentary formations. Syntectonic pluton emplacement raises the question of how to make room for magma in environments where crustal shortening, not extension, occurs on a regional scale. Finite element modeling (Nemcok and Henk, 2006) of an analogous fold and thrust belt explored for oil in the Western Carpathian Mountains of Romania showed the existence of an overall mean stress decrease inside the thrust sheet anticlines. Our interpretation asserts that in southwest Montana similar thrust sheet anticlines were also the loci of magma ascent, mineralization, and alteration processes in syncompressional environments at the top of frontal thrust ramps where “releasing steps” at ramp tops served as initial points of emplacement, subsequent pluton growth, and exceptional levels of chemical differentiation within underlying laccoliths.

Revision of the Porphyry Copper Model in the Sevier Fold and Thrust Belt

Consideration of the strong structural control on magma ascent and mineralization described above requires updating the paradigm used in porphyry exploration (fig. 2). This requires understanding features not yet well-known as a common part of the porphyry paradigm. Described here then is a revision of the tops of the porphyry copper model where the porphyry to epithermal transition might otherwise be expected (Sillitoe, 2010). Key to this revision is a distal type of early stage, high-temperature orbicular actinolite alteration shown diagrammatically here as green dots by Marco Einaudi, who along with Bill Atkinson, described the first occurrence of orbicular actinolite in diamond drill holes in the Carr Fork skarn area of the Bingham district in 1978. Since then orbicular alteration has been mapped in detail at the Clementine Prospect, and also noted at Escondida and El Hueso (Chile), Cajamarca (Peru), Morenci and Fortitude (USA), Cananea (Mexico), and Oyu Tolgai (Mongolia) (Marco Einaudi, oral commun.). Orbiclues are spherical to elliptical objects in three dimensions, often 1 to 2 cm in diameter. Orb zones are not orbicular granites nor miarolitic cavities, nor strange metamorphic effects. The orbs we have mapped at Clementine occur in the hanging wall anticline of the frontal Sevier Thrust. Since they dip outwards, we interpret them to be the Apex of a deep intact, uneroded porphyry Cu deposit. The location of orbicular alteration is shown diagrammatically in figure 2A, surrounding an ore-forming magma ascending from the top of a laccolith where magmatic water saturation occurs and drives advection fluid flow. The orb ring represents the outer edge of advective flow where radial diffusion becomes visible at crack tips and is hence mappable (Brimhall, 2018). Radiometric dating of hydrothermal titanite (70/7 +/- 1.3 Ma) was reported by Brimhall and Fanning (2019).

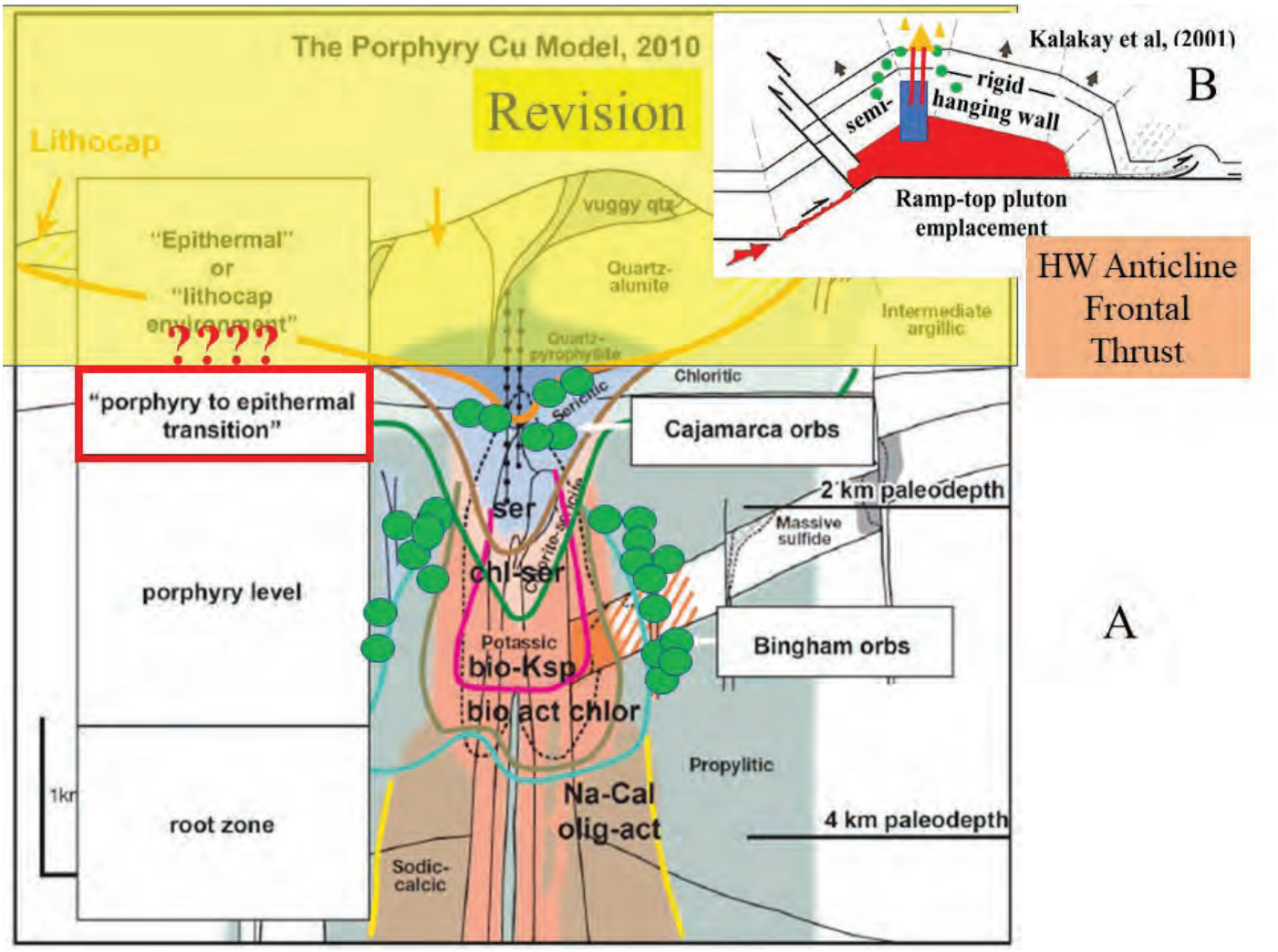

Figure 2. (A) Cross-section of porphyry copper model (fig. 6 in Sillitoe, 2010) with orbicular actinolite alteration at Bingham, Utah shown diagrammatically as green circles by Marco Einaudi (oral commun.). (B) Idealized cross-section of Kalakay and others (2001) with the proposed site of water saturation at the apex of a differentiated laccolith shown in blue, veins in red lines, and breccia in yellow triangles by Brimhall (this communication) with orbicular actinolite alteration shown as green dots.

Revisions of porphyry copper models used in exploration (Lowell and Guilbert, 1970; Gustafson and Hunt, 1975; John and others, 2010; Sillitoe, 2010) are necessary now for three reasons. First, adapting these models to a specific tectonic environment is necessary in order to reasonably estimate the likely vertical position of the present land surface within the mineralization-alteration column, since high degrees of rapid erosion (Dilles and Scarberry, this volume) are likely and porphyry deposits form over a 10-km range in depth of the emplacement (John and others, 2010; Seedorf and others, 2005). This vertical positioning estimate affects the estimates of mineral potential in grassroots, early stage, and advanced targets. Therefore, recognizing the PCD tops versus the bottoms is vital to exploring for deep mineralization systems with sound economic potential. Second, the poor discovery rate of the past decade of new grassroots PCD systems based on traditional field-based exploration methods has motivated the application of recently developed office-based technologies. According to Woodhead and Mathieu (2021), artificial intelligence (AI) has been touted as:

> "a disruptive technology that can be leveraged to reverse the current decline in discovery of quality resources. Part of this rationale stems from the belief that unrecognized or untested ore deposit signatures are likely to be present within the voluminous geoscience data that are now widely available to the public or, in some cases, reside in company archives. Artificial intelligence technologies provide an attractive way to cope with the multidimensional nature of exploration and increasingly large data sets that are routinely generated in the exploration process. In the view of the proponents of AI, this process offers the potential to quickly and efficiently extract, categorize, and analyze such data to identify the hidden signatures of ore deposits that are not readily revealed, or were missed, by conventional methods and thereby allow for more rapid testing of targets and, ultimately, an improved discovery rate."

Here, then, we caution that for AI to actually deliver on its promise, the geo-spatial PCD models into which voluminous multicomponent data is applied must be geologically accurate and relevant to specific tectonic regions to be explored. The USGS has long maintained regional studies vital in informing model development and assessment through AI: Hildenbrand and others (2000); Pearson and others, (1992); and Ruppel and others (1993). Third, deep underground mining of an enhanced resource combining PCD mineralization with bedded phosphorite with REEs and Leadville style high-grade veins and mantos provides transformational opportunities for re-imagining underground space utilization during the mine life cycle. Besides bulk mining methods of the main PCD ore body, selective mining could offer unprecedented advantages for mining REE and phosphate and stoping high-grade veins and mantos that create valuable open space for underground storage of development waste rock early in mine development. Processing wastes could be re-emplaced underground for rock support (Underground Engineering for Sustainable Urban Development, 2013).

Plan Map of the Clementine Prospect in Southwest Montana

Given the worldwide application of the Sillitoe (2010) PCD model over the past two decades of exploration, Brimhall (2018) raised the question as to what features, besides lithocaps, may prove to be effective guides to locating the porphyry copper hypogene mineralization center, particularly in the Sevier fold and thrust belt. Orbicular actinolite alteration offers new insight as it has been shown to occur not only at Bingham, Utah where it was discovered (Atkinson and Einaudi, 1978), but now also has been mapped regionally at the Clementine prospect in southwest Montana. By considering distal orbicular actinolite alteration as an early high-temperature zoning feature in both an early syntectonic Sevier age ore system at Clementine and Bingham, which formed after the Sevier orogeny, this alteration has been shown to define the outer edge of early advective fluid flow. This paper describes our fieldwork at the pre-deep pilot drilling phase to map and interpret extensive orbicular alteration as part of lateral and vertical zoning at the Clementine prospect, a possible new deep porphyry copper system in Montana. The intent is to develop within the porphyry copper paradigm new predictive mapping tools for better locating the edges and tops of hypogene hydrothermal fluid flow that has evaded many recent exploration efforts searching beneath lithocaps.

The Clementine prospect (fig. 3A) occurs between the southwest edge of the Boulder Batholith and the northernmost pluton of the Pioneer Mountains, the Big Hole River pluton. Actinolite–calcite–titanite-filled orb zones shown in circles demark a zone 3 by 5 km centered on the apex of a doubly plunging anticline where a vein breccia gossan system extends 1.5 km north–south, shown in figure 3 as thin red lines. The rock matrix be-

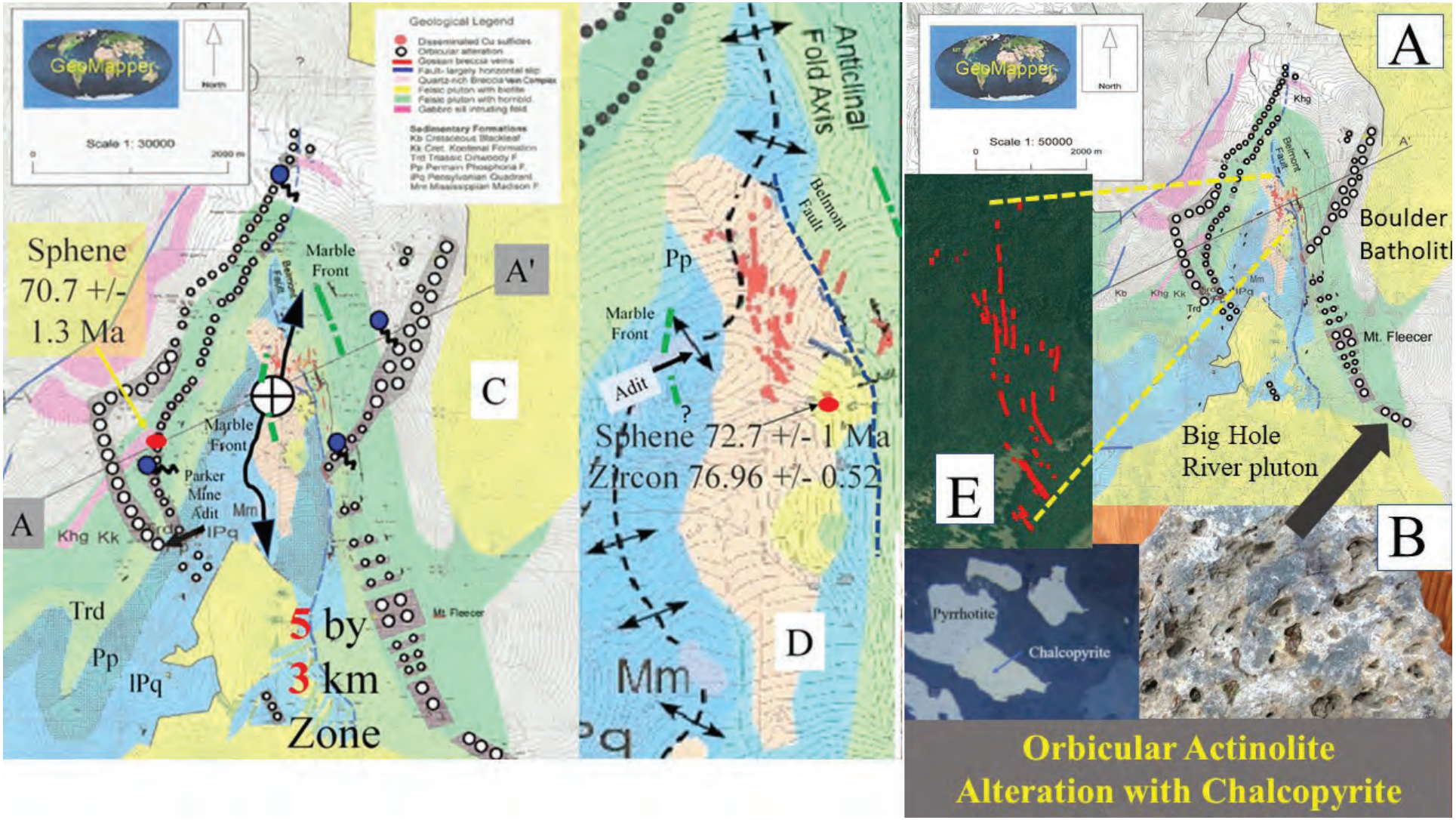

Figure 3. (A) Location of the Clementine prospect in southwest Montana between the southwest edge of the Boulder Batholith and the most northerly pluton of the Pioneer Mountains, the Big Hole River pluton. (B) Photograph of orbicular actinolite alteration shown in A with the insert showing chalcopyrite, pyrrhotite, and ilmenite between orbs zones. (C) Geological map showing the apex of the Clementine doubly plunging anticline co-axial with the surrounding actinolite orbicular rings and central zone containing a breccia vein gossan system shown in red (insert B in reflected light), 2.2-km-long elliptical zone containing barren breccias in pink, and two small plutons in yellow just east of horizontal bedding symbol. The marble front is shown in a thick green line (Sillitoe, 2010) on the east side of the anticline and a green line on the west side where it has been approximately located. It is important to note that the orbicular actinolite bands occur outside of the marble front, implying a lower temperature; yet actinolite growth is related to the early high-temperature potassic alteration expected at the deposit interior. A SHRIMP date on titanite in the orbs is shown. Blue circles are modern day springs. Cross section A–A' line trends northeast. (D) A blow-up of C with SHRIMP dates on the northern altered pluton. (E) An orthoimage of the central breccia vein gossan system mapped as red lines using digital mapping methods (Brimhall, 2018) in dense forest cover while using digital mapping methods and GeoMapper/PenMap software (Brimhall and Vanegas, 2001; Brimhall and others, 2002, 2006). Note that the breccia vein gossans are centrally located and co-axial with the outline of the orbicular actinolite zonation that defines an outer alteration ring (Brimhall, 2018; Brimhall and Fanning, 2019). Both the breccia vein gossans and orbicular alteration are mappable using digital field methods using 72-channel GNSS systems even under the densest forest canopy by combining American GPS and Russian GLONAS satellite coverage.

tween the actinolite–calcite–titanite orbs (fig. 3B) contains disseminated chalcopyrite, pyrrhotite, and ilmenite. Figure 3C shows the location of a SHRIMP radiometric age date on titanite from within an actinolite orb is 70.7 ± 1.3 Ma (Brimhall and Fanning, 2019). An enlargement of the orbicular ellipse elongated north–south (fig. 3C) shows that it is centered on and coaxial with a doubly plunging anticline. Modern-day springs that are commonly headwaters for spring creeks and mud holes are shown in blue circles with a squiggly tail. The area otherwise is remarkably dry and devoid of surface water except for late spring snowmelt runoff. Orbs define a key hydrodynamic boundary at the outer edge of early high-T hydrothermal convection and today control the aligned distribution of spring creeks. Springs and spring creeks are very rare hydrogeological features. The springs are not just random places where water flows out of the earth. The crest of the elliptical dome is centered on a 2.2-km-long elliptical zone shown in pick oriented north–south containing rock fragments of barren quartzite breccia and quartz rock flower. The marble front where the interface of dark bluish limestone is in contact with coarse-grained white marble is shown as green lines near the anticlinal crest symbol (Sillitoe, 2010, fig. 6). A further enlargement (fig. 3D) shows this anticlinal apex core area and the crest line of the anticline with a small area of Mississippian-age Lodge Pole Madison limestone near where the adit symbol is shown. Rocks on the adit mine dump contain wollastonite and marble. The marble front is shown as a dashed green line. Hence, given the observation of Meinert (1982) at Cananea, Mexico on the occurrence of wollastonite near the marble front suggests that the presence of wollastonite in marble implies prograde skarn formation at temperatures within the wollastonite stability field. Experiments by Greenwood (1967) show this temperature to be 400–450°C in fluids that are mostly H_2O with little CO_2. Shown as a swarm of red lines is a mineralized matrix breccia vein gossan system. The breccia vein gossans are not obvious continuously outcropping features but rather subtle individual samples mapped on the forest floor (fig. 3E) using 2.5-m accuracy GPS and GNSS-supported digital mapping systems described in Brimhall (2018). Only by connecting the dots of mapped vein gossan samples does their linear connectivity emerge and reveal the vein gossans as an organized system, clearly different from the barren rock breccias that occur randomly within the area (shown in pink in fig. 3D). The highest assay values of 34 vein gossan surface samples (in ppm) are: 861 Cu, 0.68 Ag, 60 Mo, 3,730 As, 2,030 Sb, 3,040 W, and 77 Ga. The breccia vein gossans are highly ferruginous, containing up to 32% Fe, reflecting a high pre-oxidation total sulfide content. Since W correlates highly with Fe (R = 0.79) and not with Ca (R = 0.23), the likely tungstate is ferberite ($FeWO_4$) rather than scheelite ($CaWO_4$), and no UV fluorescence has been observed. Ag, As, Sb, W, and Ga all correlate with Fe with R values of 0.68, 0.81, 0.97, 0.79, and 0.79, respectively, indicative of original sulfide host minerals. Ga correlates with W (R = 0.93), not Al nor Zn. Ge correlates with Ga (R = 0.78). Two small felsic plutons, each about 700 m in diameter, are shown in yellow (fig. 3). Two SHRIMP radiometric age dates on the northern pluton are shown. A hydrothermal alteration titanite gives an age of 72.7 ± 1 Ma and an older zircon age of 76.97 ± 0.52 Ma, indicating that this pluton was not the parent for the observed zoning pattern.

Permian Age Retort Member of the Phosphoria Formation

Given the fact that phosphate is now on the Critical Minerals list, one economically notable platform sedimentary wall rock formation occurring at Clementine is the Permian Age Retort member of the Phosphoria Formation, labeled Pp (shown in fig. 3C in blue with a faint stippled pattern that wraps around the anticline). The Phosphoria Formation occurs on both the west and east sides of the anticline, spanning a strike length of about 6 km. The thickness of the Phosphoria is usually less than 100 m.

Geological Cross-Section

A geological cross-section along line A–A' in figure 3C is shown in figure 4A based on surface geological mapping and formation thickness. Figure 4B shows the cratonic sequence stratigraphy defining five intercontinental unconformities from figure 1A. Actinolite–calcite orbs (fig. 4C), central vein gossan system, and an altered pluton are shown. Purple is a gabbroic sill. Four regional unconformities, each with possible paleo-karst that could have controlled formation of copper–silver mineralization, are shown as black squiggly lines. The marble front is shown as a green line. Inside the marble front proximal Cu skarn mineralization could occur, while outside the marble front distal Cu-Ag veins and carbonate replacement ore could occur. For scale, a pro-

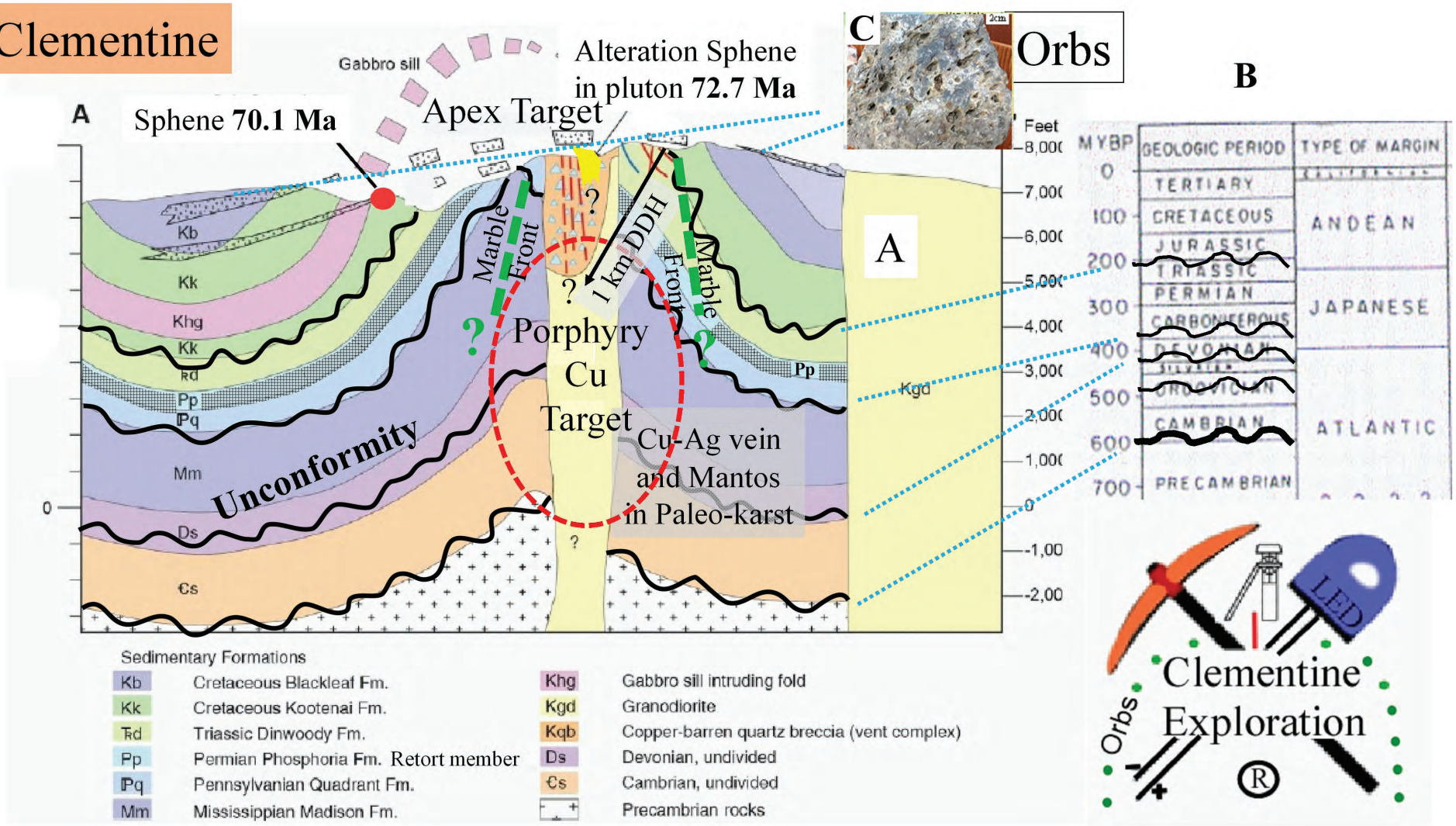

Figure 4. (A) Geological cross-section of the Clementine prospect anticline along line A–A' (fig. 3C) looking northward. The orbicular actinolite alteration is shown dipping outwards B. The central zone breccia vein gossans are shown as thin red lines. Four unconformities named in figure 1 are shown as squiggly black lines and shown in C. Paleo-karst is possible on all these unconformities. Within the near-field of the magmatic-hydrothermal system Leadville style Cu-Ag veins and mantos mineralization is possible. A proposed 1-km-long pilot diamond drill hole is shown into the apex target, probably deep enough to encounter the top of the Devonian Jefferson Formation.

posed 1-km-long drill pilot hole is shown. The Phosphoria formation (Pp) is shown with a stippled back pattern.

The local outward dip of the actinolite orbs is implied from the trace of the orb belts and how they intersect topography. These outward dips compared to the steep distal orb at Bingham imply that the present earth surface at Clementine is high in the mineralization system. This assertion is strengthened by the fact that the marble front (shown as a green line, fig. 4) can be found and mapped on the eastern-central side of the anticline. Alternatively, if what few limestone beds occur were all marble or skarn, the exposure level would be deeper in the higher-temperature part of the mineralization column. Therefore, we conclude that current topography exposes the upper parts of the Clementine mineralization system, not the mid-levels as at Cannivan Gulch nor the distal vein and mantos systems at Quartz Hill, Hecla, and Bannack. Besides Cu-Mo-Ag in the porphyry, vein, and mantos, additional metallic resources would add value to the composite system being explored.

Critical Mineral Occurrences at the Clementine Prospect

Several metals on the Critical Minerals list occur at Clementine, including As, Sb, W, and Ga in the mineralized matrix breccia vein system. In addition, the Permian age Phosphoria Formation presents an opportunity to add an important complement of valuable high-demand REEs, many of which are supply-chain-limited. The USGS has long maintained a programmatic research mission on phosphate resources in the U.S. (Hein and others, 2014) in support of production of inorganic fertilizer. Recently, Emsbo and others, 2015 and 2016 described significant REE potential occurring within the Perman age Phosphoria Formation as offering an alternative to imports of these chemical elements, which are vital to modern electronics and sustainable energy high-field-strength magnetic components and guidance systems. Most current phosphate mining in the Western Phosphate Field is done by open-pit methods in Idaho, where relatively high-grade phosphate rocks occur near the center of the Phosphoria Basin where the Guadalupian Series Roadian Stage Meade Peak member outcrops. In Montana, near the northern edge of the basin, the slightly younger Guadalupian Series Wordian Stage Retort Mountain member occurs and was mined underground east of the Pioneer Mountains at Maidenrock north of Melrose. REE consistency within a given time horizon makes both Phosphate and REEs reliable co-products (Emsbo and others, 2015). Emsbo and others (2015, 2016) show that contained REEs are entirely hosted in francolite and are nearly 100% recoverable using the same process currently used to acid leach and produce the world's phosphate supply. In addition, the REE content in even the lowest grade of these deposits exceeds the current value of the phosphate itself. At Clementine an adit with drifts in the Retort Member Phosphoria was made in the mid-1970s in Parker Creek (fig. 3C). The *in situ* value of the REEs can be put into a porphyry copper perspective using REE assays on grab samples from that Parker Creek mine dump and on the Retort Member data contained in the Supplemental Data in the Emsbo and others (2015) paper. The *in situ* value of REEs in the Retort member of the Phosphoria Formation in southwest Montana contains from about 0.3 to 1.25% copper equivalent and the P_2O_5 phosphate contains about 1 to 1.5% copper equivalent. While the Phosphoria Formation is not among the thickest platform sedimentary units, it is continuous, and with the REE suite it contains it offers economically important opportunities for selective underground mining.

Hypogene Enrichment and the Environmental Footprint

Exploration for deep porphyry copper deposits is motivated by several factors. First, grassroots discovery of new ore bodies has been a rarity in the past two decades, implying that most of the exposed systems have been discovered through traditional techniques. Such outcropping systems are exposed at their midsections in the vertical mineralization column, where relatively high sulfide content compared to their tops caused secondary supergene leaching and enrichment, creating enrichment blankets with Cu grades 2 to 5 times higher than the protore at depth (Brimhall and others, 1985a; Alpers and Brimhall, 1988, 1989). Traditionally, supergene enrichment by descending solutions provided an economic boost to the early stages of PCD mine development, making them feasible and mineable by open-pit mining methods. Today, however, environmental considerations, especially on public lands, require underground mining of deep ore bodies with a far smaller environmental footprint without generating voluminous waste rock piles from stripping leach cap waste. Consequently, a second factor motivating deep mining is that a far greater degree of selectivity in fragmenting and moving a

rock mass is possible than in mining supergene enriched systems. The economics of deep underground mining is enhanced if there are high-grade zones at depth that can be selectively mined to offset development costs. Fitting this requirement are hypogene (upward flowing solutions) that may have formed multiple high-grade ore bodies at depth in the form of proximal skarns, distal skarns, Leadville, Colorado-style veins and carbonate replacement mantos controlled by unconformities and paleo-karst, and sediment-hosted distal disseminated ores.

Proximity of Regional Unconformities with Paleo-Karst to Clementine

How close to the apex of the Clementine prospects do known paleo-unconformities with paleo-karst come? Should these features with sedimentary and eustatic origins actually occur nearby, then given the lateral continuity of sedimentary strata and unconformities, hypogene enrichment may occur in the apex anticlinal core strata at Clementine. Fortunately, a nearby exposure answers this conjecture. Only 8 km south of the Clementine apex zone, the top of the Mississippian Madison Group is exposed just west of the town of Dewey (fig. 5A). Here, the upper surface of the Madison has a reddish-orange-colored discoloration due to ancient oxidation below a 30-million-year-long exposure. The caverns are obvious proof that paleo-karst developed, then burial ensued during the subsequent Absaroka marine transgression. Figure 5B shows a diagrammatic sketch of the expected paleo-karst where Leadville and Gilman, Colorado-style high-grade Cu-Ag veins and mantos are expected at Clementine. Polymetallic Cu-Ag-Au vein and mantos ore bodies controlled by paleo-karst and evaporite solution on the Absoroka age unconformity on top of Mississippian Age Leadville limestone is analogous to the exposure of Mississippian Madison in Montana (fig. 5A). In the Leadville–Gilman belt, major porphyry systems occur, including Climax and Henderson Mo porphyries of the same general age range as the manto ore bodies.

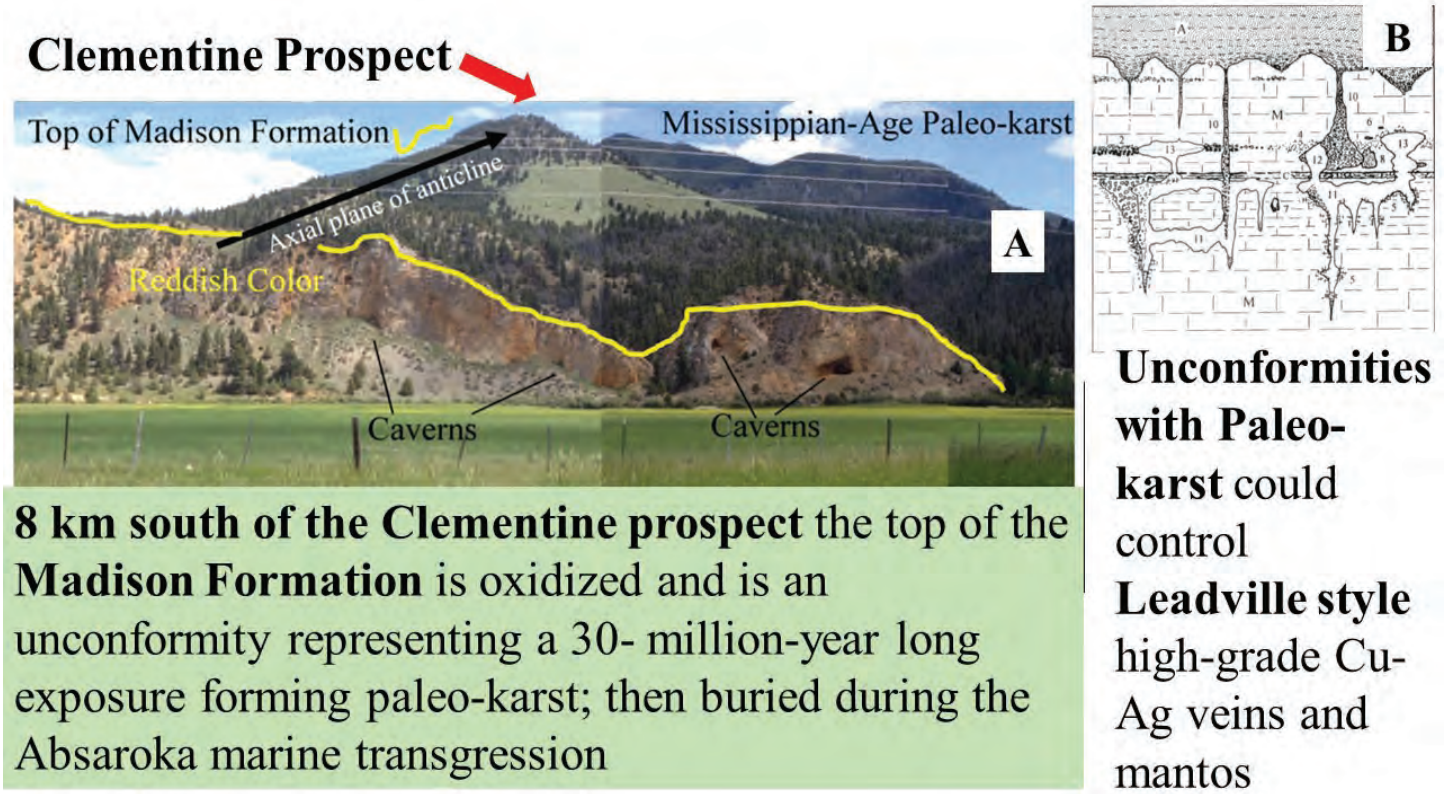

Figure 5. (A). Photograph looking north at Dewey, Montana across the Big Hole River showing the steep cliff face of the top of the exposed Mississippian Madison Group, shown as a yellow line. Reddish orange discoloration parallel to the surface of the upper formation contact is due to oxidation over a 30-million-year exposure when this surface was an unconformity. Below the unconformity surface are paleo-karst caverns. (B) Diagrammatic depiction of paleo-karst in cross-section where elsewhere in the Leadville–Gilman mining districts of Colorado, this same unconformity controlled high-grade vein and mantos replacement ore bodies.

Linking Geology with Geochemistry

Geological mapping at the Clementine prospect showed a zoning pattern similar to the Sillitoe (2010) porphyry copper model augmented with the orbicular actinolite alteration ring. The apical anticlinal dome at Clementine coaxial with the orbicular ring and central breccias vein gossan system clearly implies structural control on hydrothermal fluid flow by the Sevier age thrust and fold system consistent with the 70.7 Ma age. The McCartney Mountain stock, which intrudes the frontal fold and thrust zone east of the Pioneer Batholith and is about 30 km southeast of Clementine, has yielded a preliminary K-Ar date of 70 ± 1.5 m.y. (Ruppel and Lopez, 1984, from Brumbaugh, 1973, p. 48).

On a district scale, the orbicular alteration affects a wide variety of sedimentary lithologies within the Madison, Quadrant, Phosphoria, Dinwoody, Kootenai, and Black Leaf Formations, spanning an age from Mississippian through Cretaceous. While orbicular actinolite alteration was described long ago by Atkinson and Einaudi (1978) and noted in many porphyry copper deposits since then, the Clementine prospect appears to offer the first district-scale mapped pattern to date. Therefore, we feel it useful to understanding porphyry copper genesis broadly speaking to clarify and develop further linkages among the geology, orbicular actinolite alteration, and the overall geochemistry of the Clementine mineralization within the framework of known PCD mineral assemblages. In particular, it is vital to establish how the orbicular actinolite orb assemblages actually relates genetically to well-known porphyry copper mineral assemblages, including potassic alteration, and to granitic magmatic sources of early high-temperature hydrothermal fluids and rock buffers. Simultaneously, it is important to ascertain how orbicular actinolite alteration relates to the sedimentary wall-rock packages in the orbs that have developed.

Hydrocarbons in the Sevier Orogen

The Sevier orogenic belt and associated foreland basins include well-known hydrocarbon source rocks and reservoirs within structural traps (Ruppel and Lopez, 1984; Lageson and Schmidt, 1994). Considering also the sequence stratigraphy, unconformities, and paleo-karst where Leadville, Colorado-style replacement mantos are expected at Clementine, discerning possible geochemical relationships between actinolite orbs and mantos is important. An important clue about copper mineralized stratabound mantos in both sedimentary and volcanic rocks in north-central Chile comes from Zentilli and others (1997), where mantos contain a variety of hydrocarbons and over-mature bitumen. In order to quantify relationships of actinolite orbs with porphyry copper ore systems and stratabound copper mantos with hydrocarbons, chemical thermodynamic principles were applied to discern mineralogical relationships in the CO_2/CH_4-H_2S fluid–rock interaction framework.

Chemical Phase Equilibria

In the interest of integrating hydrothermal ore genesis with sedimentary basin evolution including hydrocarbons, a new chemical thermodynamic phase diagram of CO_2/CH_4 vs H_2S was generated by the author that compares oxidation and sulfidation states of magmatic-hydrothermal and sediment-hosted ore deposits in relation to granitic rock buffers and the sedimentary source rocks of basinal brines, hydrocarbons, and graphitic metasediments. Phase diagrams typically used to describe porphyry copper deposits cannot show hydrocarbon species, as the common coordinate axes are sulfur and oxygen fugacity without any provision for organics with carbon and hydrogen, and hence offer less than an integrated representation of sediment-hosted ore assemblages.

Equilibrium phase diagrams have long served as powerful interpretive tools for understanding the significance of recurring mineral assemblages in hydrothermal ore deposits. Holland (1959) developed the log fS_2 vs log fO_2 coordinate framework for the Fe-O-S system, which Meyer and Hemley (1967) expanded by using sulfide mineral assemblages as signpost markers demarking pathways of fluid evolution over time in relation to wall-rock alteration buffer assemblages determined petrographically and verified experimentally. Einaudi (1977) applied these phase diagrams to the Cerro de Pasco ore deposit of Peru. Brimhall (1980) added the biotite–potassium feldspar–Fe oxide buffer of potassic wall-rock alteration and showed the position of diverse early high-temperature porphyry copper systems. While log fS_2 and log fO_2 variables contributed much to advanc-

ing understanding porphyry copper ore genesis, their fugacity values are vanishingly small in magnitude and hence are not themselves major constituents in the ore-forming fluids. In the interest of representing equilibria in terms of more abundant aqueous and gas species in nature, Brimhall (1980) developed a phase diagram with log a(Fe^{2+}/a^2Cu^+) versus log fH_2S gas, which has the distinct advantage of using variables directly involved in sulfide precipitation and copper leaching (fig. 6). At different log fH_2S values serial cross-sections of log fO_2 vs log a (Fe^{2+}/a^2Cu^+) depicted the three-dimensional volumes of chalcopyrite, bornite, chalcocite, covellite, pyrite, and pyrrhotite in relation to the biotite–potassium feldspar–Fe oxide oxygen fugacity buffer (fig. 7). Recently Mernagh and Bastrakov (2013) developed the diagram of log f CO_2/CH_4 vs log fH_2S coordinates around the magnetite–pyrrhotite–pyrite assemblage, making it possible to study vapor-rich fluid inclusions using Raman spectroscopy to estimate H_2S concentrations directly.

In the present study coordinate axes of log f CO_2/CH_4 vs log f H_2S are selected again in figure 8 so that: (1) equilibria involving hydrocarbons can be added, (2) minerals formed from fluids derived from sedimentary host rocks can be depicted in the same space as magmatic-hydrothermal ore deposits, and finally (3) the relative abundance of CO_2, CH_4, and H_2S gases inferred from fluid inclusions in different types of ore-forming systems become evident in the coordinate space chosen. An advantage of using log fH_2S gas with a range of -4 to +2 in figures developed below, which is far higher than the values of log fS_2 (-5 to -8), signifies that H_2Sgas is among the abundant species in the natural systems. Furthermore, from an equilibrium of $H_2S_{gas} = H_2S_{aqueous}$ we show that $H_2S_{aqueous}$ is a major reduced sulfur species in ore-forming solutions from which sulfides precipitate. In so doing, a comparative phase diagram emerges here in which a wide spectrum of ore deposit types can be plotted

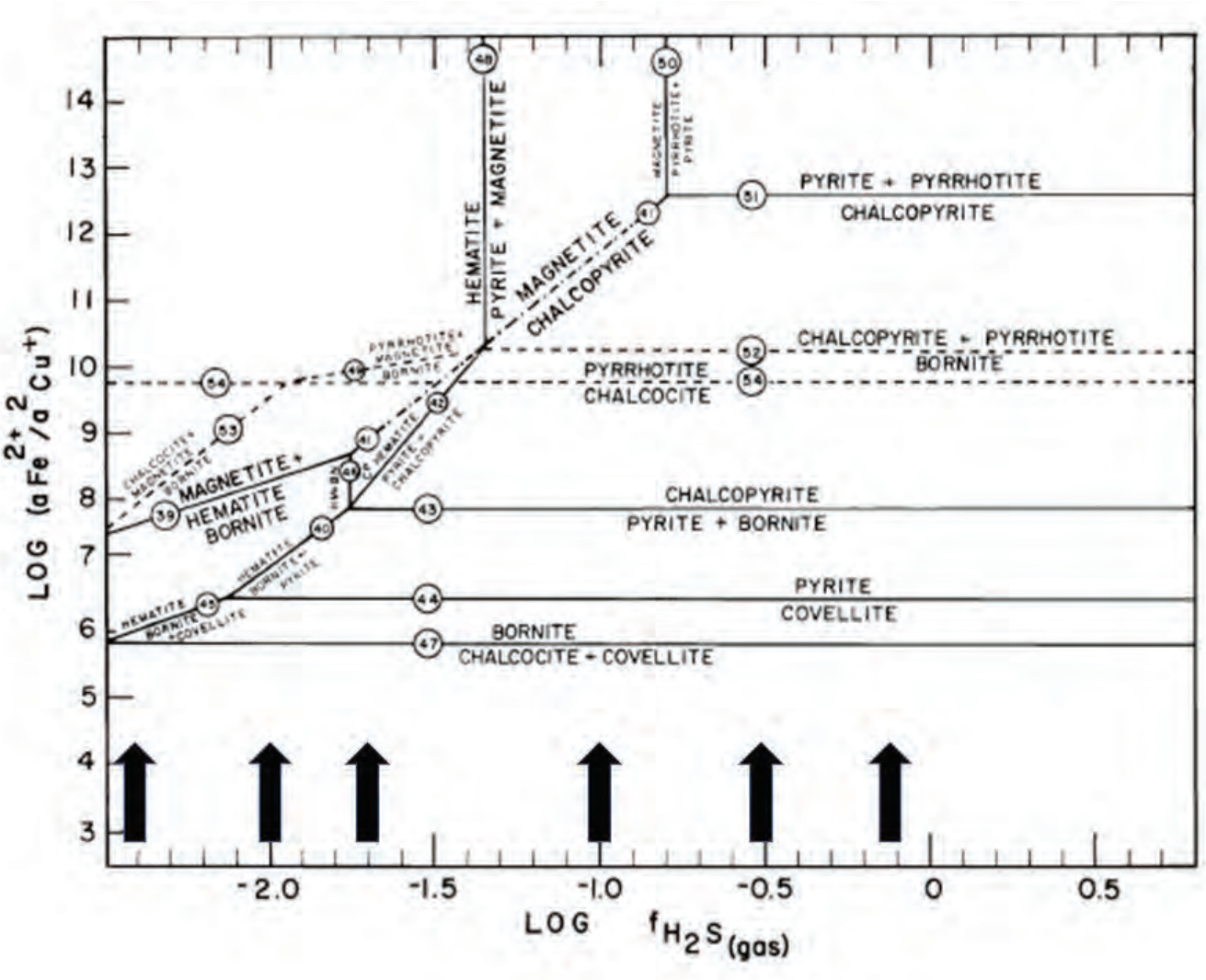

Figure 6. Mineral triple points from Brimhall (1980), figure 4, with black arrows at values of H2S for serial cross sections in figure 7.

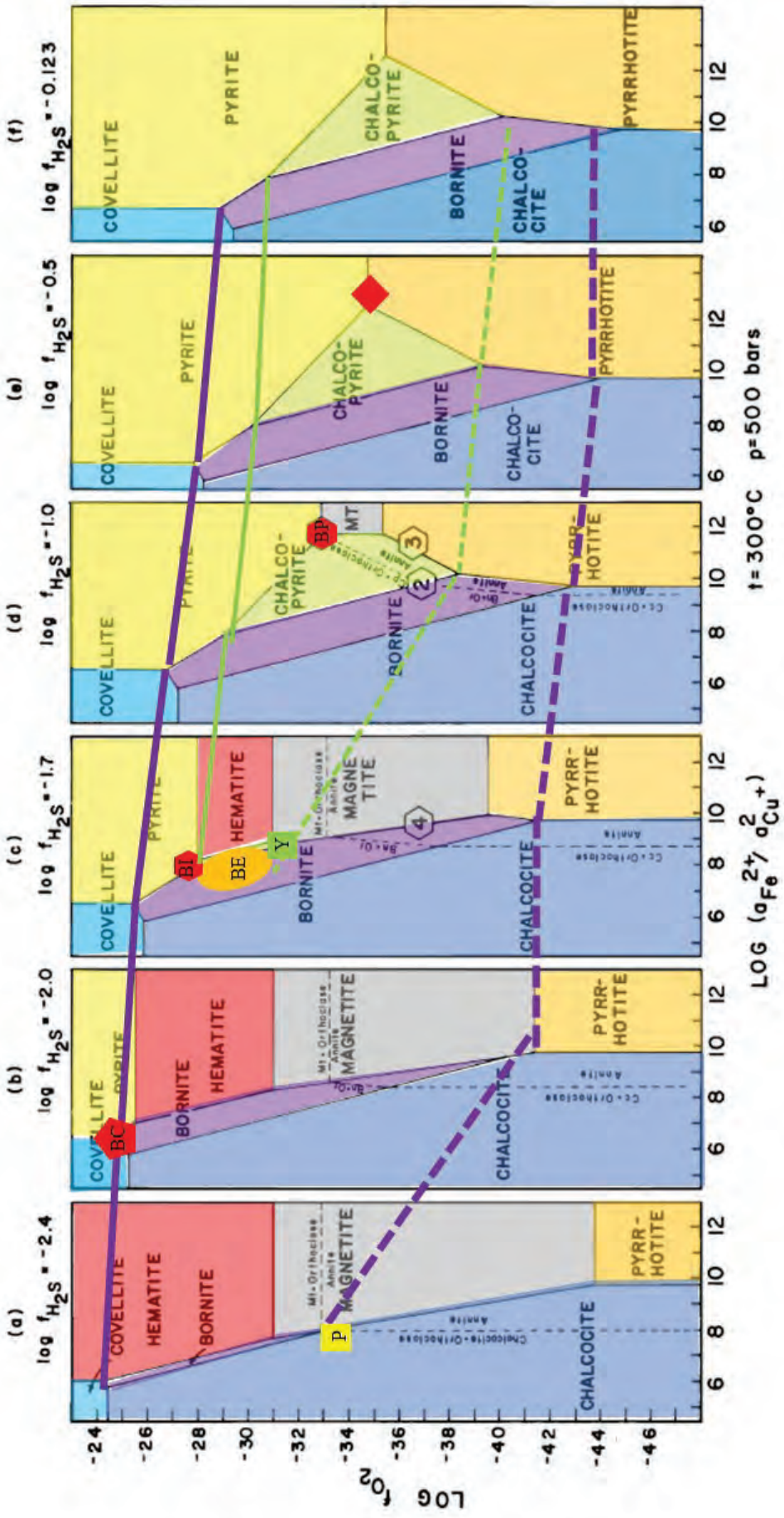

Figure 7. Serial cross-sections at different values of H2S showing the stability fields of chalcopyrite, pyrite, pyrrhotite, bornite, chalcocite, and covellite. The granite redox buffer is shown in a thin dashed line (annite–orthoclase). Mineral assemblages of porphyry copper deposits are shown: early stage Butte as red octagon (BP), intermediate zone (BI), and central zone late stage as red pentagon (BC). Pyrrhotite locked in pyrite at Butte and El Salvador Chile as red diamond. Porphyry copper assemblages from table 4 of Einaudi and others, 2003 are shown as: early chalcopyrite–bornite without pyrite or magnetite at Bingham as orange ellipse (BE). Panguna is shown in a yellow square (P) and Yerington in a green square (Y). In solid green is the trace of the high oxidation edge of chalcopyrite with the low oxidation state dashed. In solid purple is the trace of the high oxidation edge of bornite with the low oxidation state dashed. These four lines are shown in figure 9 for reference.

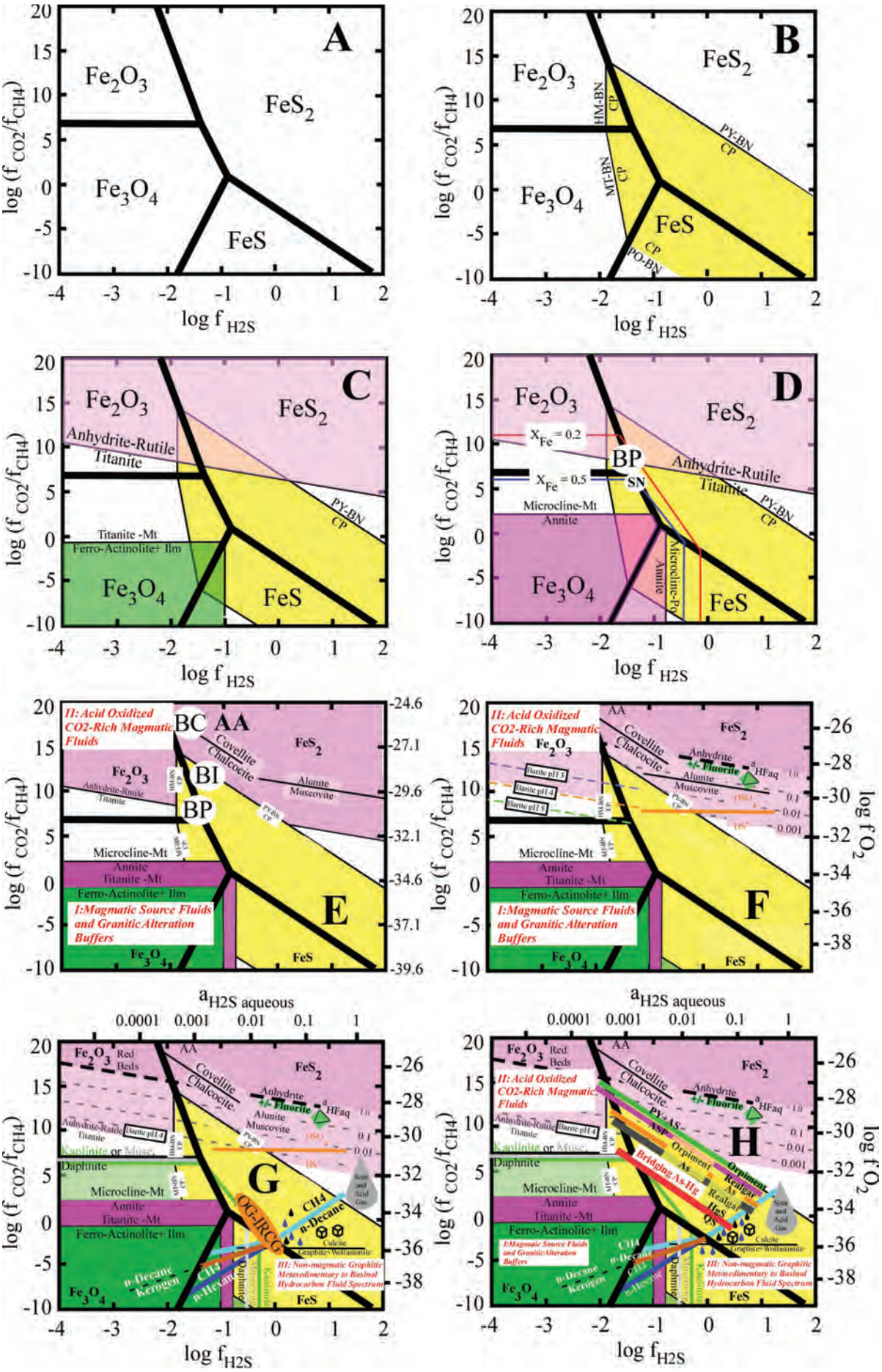

Figure 8: caption on adjoining page.

and assessed for involvement of multiple source fluids including magmatic-hydrothermal fluids, highly oxidized meteoric fluids and evaporites, and reducing sediment-derived connate basinal brines and hydrocarbons. The diagram helps to quantify geological interpretations about external fluid derivation and hypothesized mixing presented previously in schematic models of porphyry copper and related deposits (Taylor, 1974; Sheppard and Taylor, 1974; Dilles and Einaudi, 1992; Runyon and others, 2018; and Zentilli and others, 1997).

Methods

Mineral–Solution–Gas Equilibria Stoichiometry

In complex multicomponent systems, knowing which minerals occurring in rocks represent equilibrium mineral assemblages is essential to meaningful modeling and constitutes a problem to which many alternative approaches exist (Lanari and Duesterhoeft, 2019, p. 36–38). Here, rather than perform forward theoretical modeling using Gibbs Free Energy minimization (Wood, 1987), we rely on natural field and microscopic observations of well-known recurrent mineral assemblages that have been studied in ore deposits worldwide for over a century and constitute well-tested empirical features of the ore deposit models used successfully in mineral exploration (Meyer and Hemley, 1967; Hemley and others, 1980; Lowell and Guilbert, 1970; and Gustafson and Hunt, 1975). For each mineral assemblage selected, the stoichiometry of each reaction must be computed defining the reaction coefficient mole numbers for each reactant and product including CO_2, CH_4, H_2S, and H_2O. Rather than present only the final phase diagram, which is complex, the thermodynamic relations supporting different parts of the diagram are presented in stepwise stages so that the final diagram can be more readily understood (figs. 8A–8H), and readers seeking to verify and reproduce the equilibria can more easily do so. Since the coordinate axes have been deliberately chosen as log f CO_2/CH_4 vs log f H_2S, specific requirements guide how the stoichiometric coefficients are determined.

The rules developed here in determining the stoichiometric reaction coefficients are as follows: (1) conserve the number of moles of Fe and Cu in solid minerals, (2) set the coefficient of H_2S the same as the moles of S contained in sulfides, (3) in reactions where a chemical element like sulfur is oxidized, as in the formation of a sulfate-bearing mineral such as alunite, place CO_2 on the opposite side of the reaction to conserve electrons, and (4) solve three simultaneous linear equations describing conservation of mass of H, O, and C, where (5) the number of moles of CO_2 equals the number of moles of CH_4. Stipulation (3) stems from considering the oxidation (loss of electrons) of carbon in methane to form CO_2 as oxygen gas is reduced (gain of electrons) to oxide in water, whereby a total of 8 electrons are transferred and must be conserved ($C^{-4}H^{+}_4 + 2O^0_2 = C^{+4}O^{-2}_2 + 2H^{+}_2O^{-2}$). Specifically, when C^{-4} is oxidized to C^{+4}, a loss of 8 electrons, while 4 O^0 are reduced to 4 O^{-2}, which is a gain of 8 electrons, sum to zero, thus conserving electrons. Stipulation (5) is necessary in order to compute log (f_{CO2}/f_{CH4}) as the y-axis in the phase diagram, which requires that CO_2 and CH_4 occur on opposite sides of each reaction and that their stoichiometric coefficients are identical but of opposite sign. An example illustrates the algebraic solutions. Consider the hematite–pyrite phase boundary in figure 8A, where thick black lines define stability fields of pyrite, magnetite, hematite, and pyrrhotite. The defining reaction is shown in equation 1, where *l*, *m*, and *n* are the desired stoichiometric coefficients of CO_2, CH_4, and H_2O, respectively, having con-

Figure 8. Construction sequence of reaction equilibria lines at temperature of 300°C. (A) Boundaries for the hematite, magnetite, pyrite, and pyrrhotite. (B) Stability field of chalcopyrite shown in yellow. (C) Stability field of ferro-actinolite surrounded by titanite and either magnetite or pyrrhotite, shown in green with the field of anhydrite shown in pink. (D) Stability annite component of biotite surrounded by microcline, pyrite, or pyrrhotite shown in purple expanded by the influence of magnesium substitution for iron expressed as mole fraction Fe. BP and SN represent the compositions of biotites in the Butte pre-Main Stage and Sierra Nevada batholith, respectively. (E) Shows the nested fields of ferro-actinolite and annite representing I. Magmatic source fluids and granitic alteration buffers. The locations of mineral assemblages of the Butte Intermediate (BI) and Central Zones (BC) representing II. Acid-oxidized CO_2-rich magmatic fluids. (F) Fluorite–anhydrite equilibria are shown at different values of HF aqueous up to a value of 1.0. Location of barite at different values of pH. (G) Kerogen (brown), hexane (dark blue), and decane (light blue) siderite equilibria representing fluids derived from sedimentary source rocks host petroleum, gas mixtures, basinal brines, and graphitic metasedimentary fluids under reducing, CH_4 -rich conditions. (H) Bridging the sedimentary fluid source spectrum and porphyry copper/IOCG trend is a family of parallel equilibria involving quicksilver, cinnabar, arsenic, orpiment, realgar, and arsenopyrite along which basinal $H2_S$-rich petroleum/brines comingle with oxidized heated magmatic fluids. From low to high H_2S values, these bridging reactions demark hot spring Hg-Au, including the McLaughlin and Culver Baer deposits in California and Carlin Au in Nevada.

served Fe in hematite and pyrite and then set the coefficients of H_2S to a value of 4 since 2 moles of pyrite has 4 moles of S.

$$Fe_2O_3 + 4H_2S + lCO_2 = 2FeS_2 + mCH_4 + nH_2O. \quad (1)$$

Conservation of the number of moles of H, O, and C is given by equations 2, 3, and 4, respectively.

$$8 = 4m + 2n, \quad (2)$$
$$3 + 2l = n, \text{ and} \quad (3)$$
$$l = m. \quad (4)$$

Solving equations 2, 3, and 4 simultaneously gives $l = m = 0.25$ and $n = 3.5$, as shown in equation 5.

$$Fe_2O_3 + 4H_2S + 0.25CO_2 = 2FeS_2 + 0.25CH_4 + 3.5H_2O. \quad (5)$$

Notice that the rules stated above are followed since CO_2 and CH_4 are on opposite sides of the reaction and that their stoichiometric coefficients are both 0.25. Notice also that there are 2 moles of Fe in both Fe_2O_3 and $2FeS_2$. Finally notice that there are 4 moles of S in both $4H_2S$ and $2FeS_2$.

Example of Equilibrium Expressions

With the activity of H_2O set to 1 for simplicity, the equilibrium constant for equation 5 is given in equation 6 as:

$$K = \frac{f_{CH4}^{0.25}}{f_{CO2}^{0.25}} \frac{1}{f_{H2S}^{4}} \quad (6)$$

Taking logarithms yields a linear equation for the magnetite-pyrite phase boundary in equation 7

$$\log \frac{fCO2}{fCH4} = -16 \log f_{H2S} - 4 \log K \quad (7)$$

The value of log K is computed as 3.826 as described below yielding a linear equation in the general form of $y = a_o + a_1x$ as given in Eq. 8 where the y-intercept is -15.305 and the slope is negative 16.

$$\log \frac{fCO2}{fCH4} = -15.305 - 16 \log f_{H2S} \quad (8)$$

Chemical Thermodynamic Calculations

The phase diagram has been computed here using thermodynamic equilibrium constants at 300°C and 50 MPa showing mineral-solution-gas reactions within CO_2/CH_4-H_2S gas fugacity coordinates. These physical conditions have been chosen so as to serve as a comparative reference condition for quantitatively describing mineral–solution–gas equilibria within porphyry copper deposits, orbicular actinolite alteration, and high-temperature oil field hydrocarbons. Once the reaction stoichiometry have been determined using the linear algebraic methods above, equilibrium thermodynamic calculations have been made using three software packages: CHNOSZ (Dick, 2019) for equilibria involving organic species and GEOPIG (Windman and Shock, 2008),

which are based on use of the SUPCRT92 package of Johnson and others (1992) developed at the University of California, Berkeley, incorporating advances in internal consistency in the database (Helgeson and others, 1978, 1998). SUPCRTBL (Zimmer and others 2016) was also used, and is based on the data contained in Holland and Powell (2011). Here, internal consistency of the thermodynamic data used has been checked by running the same chemical reaction in different computer programs.

Recurrent Mineral Assemblages

Recurrent sulfide–oxide–silicate mineral assemblages are well known in the ore deposit classes chosen for this study and in fact are an integral part of the genetic models of porphyry copper deposits and many other types of ore deposits. The reason for recurrent mineral assemblages lies in chemical thermodynamic equilibrium. In fact, recurrent mineral assemblages are proof that natural hydrothermal processes over time tend towards a state of equilibrium. Since Fe, O, and S are abundant chemical elements in ore deposits, the phase boundaries shown in figure 8A as heavy dark black lines exert a powerful buffering influence on the paths taken by ore-forming solutions seeking equilibrium. Mineral assemblages that typify several world-class ore deposits, including Butte, Montana, are plotted in the figures as they are developed in order to illustrate the use of the phase equilibria.

Chalcopyrite Stability Field

The stability field of chalcopyrite is shown in figure 8B in yellow. Chalcopyrite stability is central to understanding this phase diagram. Notice in particular that chalcopyrite has an extensive stability field situated astride the stability fields of hematite, magnetite, pyrite, and pyrrhotite, which are the most common ore-related Fe-minerals in nature. Note, however, that the chalcopyrite stability field does not occur at values of log fH_2S below -1.8, as discussed in Brimhall (1980), where detailed serial cross-section diagrams span wide ranges of log fH_2S and log aFe^{2+}/a^2Cu+, thus depicting three-dimensional volumes of sulfides in figures 6 and 7 contained therein. In figure 7 the extremities of the chalcopyrite field trace out the low and high limits of oxygen fugacity expressed here as log f CO_2/CH_4. Below log fH_2S values of -1.8, there is insufficient reduced aqueous sulfide to form chalcopyrite, although the more copper-rich but sulfur-poor sulfide bornite is stable. In the pyrite field, chalcopyrite is surrounded by bornite and in the hematite field chalcopyrite is surrounded by bornite. Similarly, in the magnetite field chalcopyrite in surrounded by bornite alone, and in the pyrrhotite field, chalcopyrite is surrounded by bornite.

Wall-Rock Alteration Mineral Assemblages

Common hydrothermal wall-rock alteration assemblages are readily depicted using the algebraic procedures described above. Here we show where in the diagram actinolitic and potassic alteration occurs in relation to magnetite, hematite, pyrite, pyrrhotite, and chalcopyrite. Since most hydrothermal amphiboles and biotite occur in solid solution containing iron, magnesium, and other elements, we show these phases as their iron-end members and then illustrate how incorporation of magnesium changes the phase relations using ideal site mixing in annite–phlogopite solid solutions (Brimhall and Crerar, 1987; Ague and Brimhall, 1987, 1988).

Ferro-actinolite, titanite (sphene), anhydrite, and rutile stability fields are depicted in figure 8C with the field of ferro-actinolite plus ilmenite being shown in dark green, surrounded by titanite (sphene) in both the magnetite and pyrrhotite fields. Substitution of Mg^{2+} for Fe^{2+} causes the actinolite field to expand outward so its upper right-hand corner extends into the pyrite field. The equilibria of titanite, anhydrite, and rutile is shown as occurring at high values of CO_2/CH_4 within the hematite and pyrite fields. The stability field of anhydrite is shown in pink. Titanite–anhydrite–rutile stability is important in understanding oxidizing conditions in porphyry copper deposits and is often related to biotitization of hornblende (Roberts, 1973, 1975; Brimhall and others, 1985b; Brimhall and Crerar, 1987).

The annite and microcline stability fields are shown in figure 8D, with the field of annite shown in purple surrounded by microcline plus magnetite, pyrite, or pyrrhotite. The stability field of annite expands outwards with substitution by Mg^{2+} for Fe^{2+} as the mole fraction annite (X_{Fe}) decreases from 1.0 to 0.5 and expands even more to a more fraction annite to 0.2 for highly Mg-rich hydrothermal biotites characteristic of potassic al-

teration in the porphyry copper deposits, which are both phlogopitic and highly enriched in F^- (Brimhall and others, 1985; Brimhall and Crerar, 1987; John and others, 2010) compared to common igneous biotites of the Sierra Nevada batholith "SN" (Ague and Brimhall, 1987, 1988a,b). Notice that the biotite boundary for X_{Fe} equal to 0.5 is near the triple point magnetite–pyrite–hematite and the titanite–anhydrite–rutile equilibria. The early high-temperature porphyry copper pre-Main Stage assemblage at Butte, Montana shows hornblende in the Butte granite wall rock that has been biotitized (Roberts, 1973, 1975), sphene has been converted to rutile, and anhydrite is shown plotted as a circle as "BP" although it formed at even higher temperatures (Brimhall, 1973, 1977) near 650°C. The high-Mg hydrothermal biotites are also fluorine-rich. Fluorination by late-stage magmatic volatiles is the cause of the oxidation and increase in log (f_{CO2}/f_{CH4}; Brimhall and Crerar, 1987). Brimhall (1979) and Brimhall and Ghiorso (1983) described hypogene copper leaching of the pre-Main Stage mineralization as the source of copper in the Main Stage veins.

The muscovite–alunite boundary occurs at the high levels of log (f_{CO2}/f_{CH4}) where anhydrite is stable and titanite (sphene) is unstable as shown in figure 8E. Finally at the highest levels of log ($f\ CO_2/f\ CH4$), the chalcocite–covellite boundary occurs typical of advanced argillic alteration (Brimhall, 1980). Notice in figure 8E that along the righthand edge of the figure, values of log fO_2 are shown that are calculated from the equilibria given in equation 9, for which the log K is -69.102 and the conversion of log (f_{CO2}/f_{CH4}) to log $f\ O_2$ is given in equation 10.

$$CO_2 + 2H_2O = CH_4 + 2O_2, \text{ and} \qquad (9)$$

$$\log fO_2 = -34.551 + 0.5 \log (f\ CO_2/f\ CH_4). \qquad (10)$$

The advanced argillic alteration assemblage with chalcocite and covellite represents the highest f_{CO2}/f_{CH4} and fO_2 states in porphyry ore deposits under hydrothermal conditions. The Main Stage mineral assemblage of the Central Zone of the Butte mining district in Montana (Meyer and others, 1968; Guilbert and Zeihen, 1964) is represented by point "BC" where covellite and chalcocite occur with advanced argillic wall-rock alteration (AA) with alunite (Khashgerel and others, 2008). In figure 8E notice the label in red: "I: Magmatic Source Fluids and Granitic Alteration Buffers," which applies to the lower left corner of the phase diagram. In contrast, notice in the upper left corner in red: "II: Acid Oxidized CO_2-Rich Magmatic Fluids." While oxygen is obviously a strong oxidant, it is not the strongest—a characteristic exceeded only by fluorine, which is the most electro-negative element in the Periodic Table. Consequently, the highly oxidizing advanced argillic assemblage (AA) often includes traces of fluorine-bearing minerals including fluorite (CaF_2), Zunyite ($Al_{13}Si_5O_{20}(OH,F)_{18}Cl$), and topaz ($Al_2SiO_4(F,OH)_2$) (Guilbert and Zeihen, 1964) and has cuprous sulfide ($Cu^{+1}S$) in equilibrium with covellite, cupric sulfide ($Cu^{2+}S$). The source of the fluorine in minerals of the advanced argillic assemblage is most likely the fluor-phlogopite in the district-scale Potassic alteration zone associated with the pre-Main Stage mineralization, which was dissolved and replaced by voluminous sericitic alteration during the Main Stage event.

The fluorite stability field in relation to anhydrite is expressed in equation 11, which has a log K equal to -13.473.

$$CaF_2 + H_2S + CO_2 + 2H_2O = CaSO_4 + 2HFaq + CH_4. \qquad (11)$$

Unlike that of anhydrite, the stability field of fluorite depends upon an additional variable, log a_{HF} aqueous, as shown in equation 12:

$$\log (f_{CO2}/f_{CH4}) = 13.473 - \log fH_2S + 2\log a_{HFaq} \qquad (12)$$

Figure 8F shows the bottom edge of the fluorite stability field for log a_{HFaq} values from 0.001 to the highest possible value of 1.0, where HFaq would be the dominant species in the ore-forming fluid rather than water. The iso-activity line for HSO_4^- and HS^- is shown in orange. Above this line oxidized sulfate dominates and below this line reduced sulfide occurs. Notice that high values of HFaq are within the HSO_4^- field well above the HS^- field relative to the iso-activity line shown in orange. Barite, like fluorite, has a stability dependent upon several factors, including pH and Ba^{2+} in solution. Here barite is shown for an assumed barium concentration of 100 ppm (Candela and Piccoli, 2005) for pH values of 3, 4, and 5, showing that barite, a mineral containing sulfate, plots within the HSO_4^- field where fluorite is also stable.

Hydrocarbon Reactions

Helgeson and others (2009) published a comprehensive chemical and thermodynamic model of oil generation in hydrocarbon source rocks that included thermodynamic data for solid, liquid, and gaseous hydrocarbons. Using this data, Dick (2019) created a new user computer interface called CHNOSZ that runs in R, which is an online computing environment for statistical computing and graphics. CHNOSZ computes equilibria involving organic species, consistent with the thermodynamic data of the SUPCRT92 package (Johnson and others, 1992), making it possible here to integrate into one phase diagram, organic phase equilibria with traditional inorganic species and thereby explore the possible oxidation–reduction–sulfidation relationships between different major ore-forming systems and sedimentary source rock organics and brines. While thermodynamic data in Helgeson and others (2009) does not include all the organic species identified by chromatography in ore deposits such as those described by Peabody and Einaudi (1992) or Peabody (1993), several common and geologically important species are included. In particular we compute phase relationships for mature kerogen ($C_{128}H_{68}O_7$), n-hexane (C_6H_{14}), and n-decane $C_{10}H_{22(l)}$ using the same algebraic methods discussed above that conserve moles of carbon, hydrogen, and oxygen, although the calculations are more difficult given the high molecular weights of the organic species. Figure 8G shows the phase boundary between mature kerogen and n-decane (eq. 13), n-hexane and methane (eq. 14), and n-decane and methane (eq. 15) in the presence of siderite and pyrrhotite or pyrite as in equation 16.

$$C_{128}H_{68}O_7 + 118FeS + 63\,CO_2 + 221H_2O = C_{10}H_{22}g + 63CH_4 + 118\,H_2S + 118\,FeCO_3, \quad (13)$$

$$C_6H_{14} + 6FeS + 8.5\,H_2O + 4.75CO_2 = 4.75\,CH_4 + 6FeCO_3 + 6\,H_2S, \quad (14)$$

$$C_{10}H_{22(l)} + 10FeS + 14.5\,H_2O + 7.75CO_2 = 7.75\,CH_4 + 10FeCO_3 + 10\,H_2S, \text{ and} \quad (15)$$

$$C_{10}H_{22(l)} + 10FeS_2 + 19.5\,H_2O + 5.25CO_2 = 5.25\,CH_4 + 10FeCO_3 + 20\,H_2S. \quad (16)$$

High values of H_2S fugacities are referred to as “sour” gas in the petroleum industry and reach levels as high as 40 percent of the gas phase (Gong, and others, 2014). CO_2-rich gas is referred to as “acid” gas. Both extreme gas concentrations are shown diagrammatically in figure 8G in a gray bubble. In the sour gas region where the log H_2S gas values are around 1.2, the activity of aqueous of H_2S (not log) can be calculated from the equilibrium constant for the equilibria of H_2S_{gas}=$H_2S_{aqueous}$, which is -1.568. Therefore, although the log H_2S gas fugacity is about 1.2, the log activity of aqueous H_2S is much lower, with a value of -0.368 or an activity of 0.42, implying that the associated fluid is still aqueous but with a high aqueous H_2S concentration. The scale of a $H_2S_{aqueous}$ is plotted along the top of figure 8G.

Chlorite–Muscovite–Kaolinite Reactions

Notice that these organic phase boundaries above intersect the annite–microcline boundary in the lower-left corner of the diagram in the pyrrhotite and magnetite fields typical of reduced granitic rocks. Surrounding the

granitic rock buffer, several other silicate mineral buffer reactions involving chlorite, muscovite, and kaolinite are important in sedimentary source rock environments and also as hydrothermal alteration reactions, but at higher values of log f CO_2/CH_4 and lower values of H_2S fugacities than in sedimentary environments. Phase boundaries for the Fe-end member chlorite (daphnite) with the clay mineral kaolinite are shown in light green and with muscovite in gray. Chlorite precipitation may inhibit quartz infilling pore and cracks and thereby maintain and enhance permeability in deeply buried sandstones (Worden and others, 2020) from which pore fluids may escape that become ore-forming non-magmatic brines.

Calcite–Graphite–Wollastonite Reaction, Orogenic Gold Deposits, and the Source of Water

Intersecting both the organic phase reactions and the daphnite to muscovite or kaolinite reactions is an equilibria involving calcite–graphite–wollastonite, shown in the lower right corner of figure 8G cutting the pyrite–pyrrhotite phase boundary. This assemblage of pyrite–pyrrhotite with graphite and wollastonite reflects the interpreted upper limit of orogenic gold deposits (Tomkins and Grundy, 2009) and the computed log f CO_2/CH_4 vs log f H_2S coordinates of both the Missouri gold deposit in Western Australia (Mernagh and Bastrakov, 2013) and the mineral assemblage in the "Reduced" porphyry copper–gold deposits described by Rowins (2000), labeled in figure 8G as "OG-IRCG." Finally, notice that in the lower right corner of figure 8G, a new label is shown in red: "III: Non-magmatic Graphitic Metasediment to Basinal Brine Hydrocarbon Fluid Spectrum."

Mercury–Arsenic Mineral Equilibria: Geochemical Bridge Pathways to Sediment-Hosted Ore Deposits

In figure 8H, equilibria involving sulfide minerals containing Hg and As (quick silver, cinnabar, realgar, elemental arsenic, orpiment, and arsenopyrite) form a family of parallel lines with a negative slope connecting two disparate stability fields: "III: Non-magmatic Graphitic Metasedimentary fluids and Basinal Brine Hydrocarbon Fluid Spectrum" and "II: Acid Oxidized CO_2-Rich F-Rich Magmatic Fluids." The implications of the Hg-As mineral reaction lines are obvious and powerful. These equilibria with quicksilver, elemental arsenic, realgar, orpiment, and arsenopyrite bridge a large geochemical space transitional between petroleum source rocks and epithermal veins with reduced (HS^-) sulfur species where gold transport occurs with magmatic-hydrothermal systems (Hofstra and Cline, 2000). These equilibria involving Hg and As minerals provide a family of reaction pathways buffered by coexisting As and Hg minerals connecting sediment-derived fluids with magmatic sources of heat and aqueous fluids, thus making interactivity of disparate metallogenic systems inevitable when and where geological proximity and permeable pathways develop.

Results

Assembly of the chemical thermodynamic reactions for sulfide, oxide, silicate alteration mineral, and organic petroleum liquids and gases shown in figures 8A–8H are assembled in figure 9. Most importantly, three distinct end member fluid compositions contributing to ore deposition are shown in red text: "I: Magmatic Source Fluids and Granitic Alteration Buffers" (lower left), "II: Acid Oxidized CO_2 and F- rich Magmatic Fluids and/or Meteoric water," and "III: Non-magmatic Basinal Brine Hydrocarbon Fluid Spectrum" (lower right).

Porphyry Copper Deposits

In figure 9 several key mineral assemblages of the district-scale zoning of the Butte mining district in Montana described in Meyer and others (1968) are depicted and labeled: "Butte Trend" shown with a diamond checkboard trend. Red ellipse "BP" represents the early high-temperature pre-Main Stage porphyry copper mineralization at Butte, Montana (Brimhall, 1977) at the triple point of magnetite–pyrite–hematite with chalcopyrite near the Mg-rich biotite–microcline granite buffer and the triple point magnetite–pyrite–chalcopyrite shown in Brimhall (1980, fig. 5). Here, potassic alteration involves biotitization of the hornblende of the Butte Granite forming a Mg-rich hydrothermal biotite (Robert, 1973,1975; Brimhall, 1977; Brimhall and others, 1985; Brimhall and Crerar, 1987) coexisting with rutile and anhydrite shown along the lower edge of the anhydrite stability field, shown in pink. "BI" represents the Butte Intermediate Zone (Meyer and others, 1968; Guilbert and Zeihen, 1964) with high-grade Main Stage copper veins consisting of chalcopyrite–pyrite and chalcopyrite–bornite veins with sericitic alteration envelopes that locally destroyed the granitic wall-rock buffer and allowed the

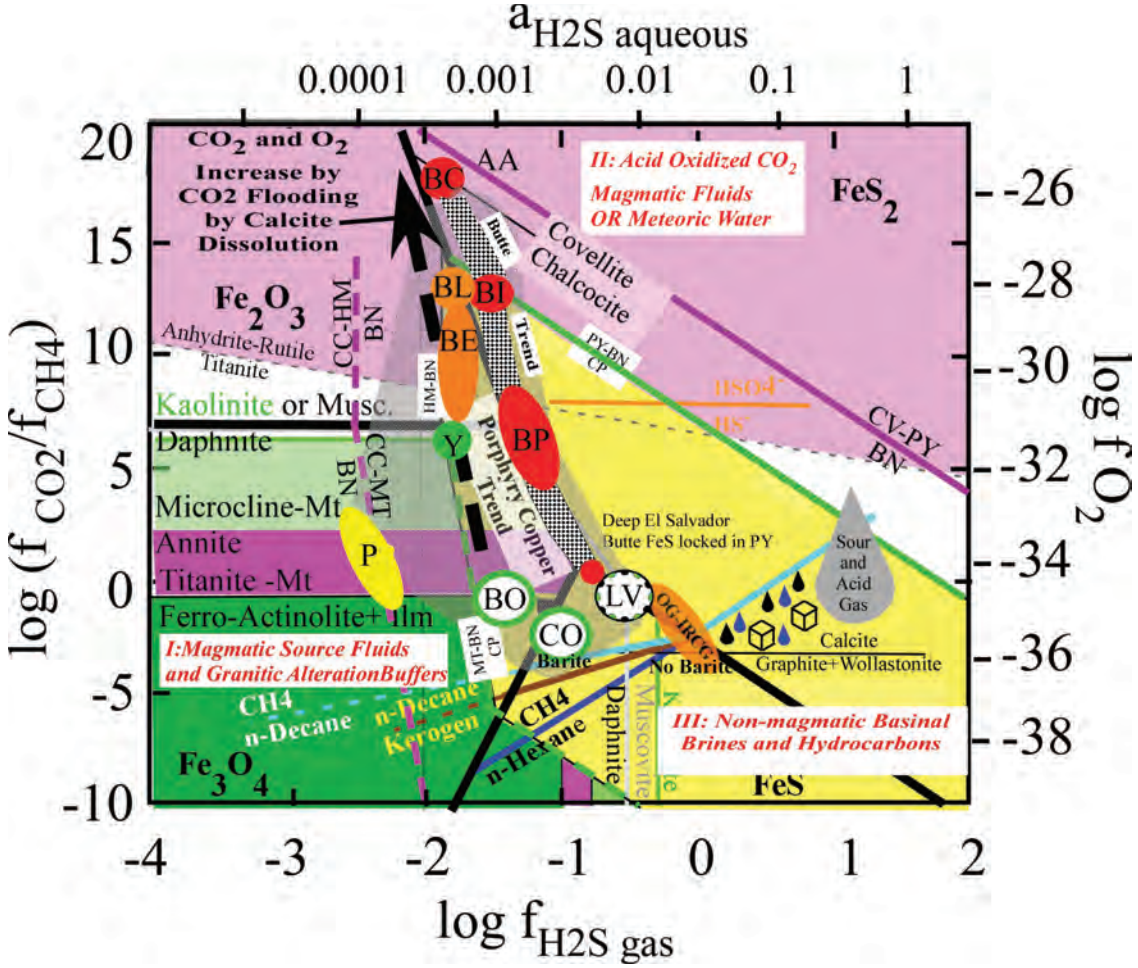

Figure 9. Color patterns are as follows: dark green represents actinolite, purple represents biotite, and light green represents chlorite in granitic magmas and related hydrothermal wall-rock alteration mineral assemblages defining reducing, low H2S conditions. Pink represents anhydrite either as a hydrothermal mineral or in evaporite sediments. Black oil droplet and cubes represent the hydrocarbon and salt brines emanating from sedimentary basin source rocks by diagenesis and maturation of organic carbon. Notice that these symbols occur near brown (kerogen) and blue (n-decane and n-hexane to methane) equilibria for petroleum products. Porphyry copper deposits shown in stipples define a nearly vertical band in which the Butte pre-Main Stage (BP), Intermediate Zone (BI), and Central Zone (BC) with covellite–chalcocite and advanced argillic alteration (AA) and alunite occur, forming the Butte Trend line, shown as a diamond checkerboard pattern. Other porphyry Cu deposits shown are Yerington (Y) and Panguna (P). Orbicular actinolite alteration at the Bingham Mine in Utah (BO) and the Clementine Prospect in Montana (CO) are shown as circles with a green rim and fall on the stippled porphyry copper trend line. Barite at Clementine proves that it is related to an oxidizing parent magma like Bingham, not a reducing magma as in the equi-granular orogenic gold-reduced cooper gold systems (OG-IRCG). The heavy black arrow depicts the effect of carbonate dissolution at depth, which drives up the CO_2/CH_4 ratio and the O_2 fugacity upwards along the granitic wall-rock and actinolite buffers, causing the sulfide mineral assemblages to evolve from pyrrhotite–chalcopyrite to chalcopyrite–bornite to bornite–chalcocite.

f CO_2/f CH_4 to rise by five orders of magnitude and the f O_2 by two orders of magnitude with incursion of meteoric water (Sheppard and Taylor, 1974). Point “BC” represents the Central Zone at Butte, Montana (Meyer and others, 1968; Guilbert and Zeihen, 1964), consisting of chalcocite–covellite–pyrite with advanced argillic alteration, often with alunite and pervasive sericite alteration that completely destroyed the buffer capacity of the Butte Granite (Brimhall, 1980). Using early mineral assemblages shown in table 4 from Einaudi and others (2003), “Y” for Yerington represents chalcopyrite–bornite–magnetite assemblages; “BE” and “BL” are for Bingham Canyon, Utah early and late sulfide assemblages. Shown as “BO” is distal orbicular Mg-rich actinolite alteration, first described by Atkinson and Einaudi (1978) in the Carr Fork area of the Bingham porphyry copper deposit. Such orbs have also been recognized at three deposits in Chile: Caspiche, La Escondida, and El Hueso; Cajamarca in Peru; Morenci and Fortitude Copper Canyon in the U.S.; Cananea in Mexico; and Oyu Tolgoi in Mongolia (Marco Einaudi, written commun.,2019). Finally, “CO” represents distal and high-level orbicular actinolite alteration with chalcopyrite, pyrrhotite, ilmenite, titanite (sphene), and actinolite at the Clementine Prospect, Montana (Brimhall, 2018; Brimhall and Fanning, 2019), mapped over a 2 by 6 km zone centered on a vein gossan system. Since Clementine has barite in sulfide assemblages, it is clear that the parental magma is

oxidizing, not reduced. Considering these data points together with geochemical evolution paths, porphyry copper mineral assemblages form a clear evolutionary trend line positioned along the hematite–pyrite and magnetite–pyrite boundaries, which coincides with a granitic wall-rock and potassic alteration buffer with Mg-rich biotite. Once oxidizing fluids interact with the early-stage mineral assemblages, the granitic rock buffer is outrun by sericitic alteration and the system evolves upwards in the diagram, where CO_2 dominates in meteoric fluids. In contrast, the reduced end of the trend has equal CH_4 and CO_2 fugacities and H_2S up to 10 times higher where distal orbicular actinolite alteration forms by diffusion at crack tips occurring along the edges of advection in porous wall-rock sediments (Brimhall, 2018). Here, rather than buffering by the potassic alteration assemblages, buffering is by ferro–actinolite–titanite–pyrrhotite.

Reaction Mechanism of Carbonate Sections of Wall Rocks on Cu and Critical Mineral Expression

Carbonate-bearing sedimentary wall rocks exert a far stronger hydrolysis effect on hydrothermal fluids than volcanic and plutonic wall rocks. Magma-derived acid attack of thick sections of carbonates produces CO_2 gas which rapidly elevates the CO_2/CH_4 ratio (eq. 9) and drives the fluid composition towards a higher oxidation state, as shown with the black arrow in figure 9 along the porphyry copper trend line. Both the Mississippian Madison (Mm) and Devonian (Dm) formations, with a combined thickness of 1,000 m (figs. 3, 4), served as external sources of CO_2 to the magmatic–hydrothermal system, forming a large open geochemical system. While the distal edges of a DASHER PCD has orbicular alteration at the base of the black arrow under a relatively low oxidation state, acid attack of the carbonate formations elevated the CO_2/CH_4 ratio and O_2 substantially from the chalcopyrite–pyrrhotite boundary up into the bornite and chalcocite fields along the edge of the granitic wall-rock and actinolite buffer boundaries. Compared to volcanic-hosted PCDs, carbonate dissolution also broadens the array of minerals precipitated so that a fuller expression of the overall suite of metals being transported from the parental magma is made possible including W, As, Sb, Ga, Te, Bi, and Se. It is possible also that dissolution of dolomite releases magnesium, which extends the solid solution range of hydrothermal biotite towards higher oxidation states and more copper-rich sulfides.

CO_2 Release by Limestone Dissolution, Causing Bornite Occurrence in Early Stage Porphyry Copper Deposits

Figure 9 illustrates an important difference between porphyry copper deposits developed entirely within plutonic wall rocks as at Butte, Montana and systems developed in wall-rock sequences containing major thicknesses of carbonates such as Bingham, Utah; Yerington, Nevada; El Salvador; Chile; Potrerillos, Chile; and Clementine, Montana. At Bingham, Utah the early sulfide assemblage with bornite and chalcopyrite (without pyrite or magnetite) is shown at point “BE” in an orange ellipse and the early bornite–chalcopyrite–magnetite assemblage at Yerington “Y” is shown in green, in contrast to the early assemblage of chalcopyrite–pyrite–magnetite at Butte “BP” in red, which lacks bornite (fig. 9). The consequence of the presence of bornite correlates with higher copper grade early stage ore assemblages than in deposits lacking early bornite as at Butte. This has a major impact on the concentration of gold as it substitutes for copper in early sulfides. Later sulfide assemblages involve incursion of meteoric water forming the intermediate “BI” and “BC” Butte Central Zone high sulfidation state assemblages with advanced argillic alteration and the Bingham “BL” late-stage chalcopyrite with pyrite (Marco Einaudi, written commun.). In summary, while admixture of oxidizing meteoric water may extend the oxidation trend considerably, the starting point with respect to the presence or absence of bornite may instead reflect incursion of CO_2-rich gases released from limestones at depth undergoing dissolution. Furthermore, while the redox state of parental magmas plays a role, the presence of a reactive carbonates in the wall-rock stratigraphic section also plays a determinative role in setting the early sulfide assemblage, copper, and gold grades.

Reduced “porphyry” copper–gold deposits described by Rowins (2000) are viewed by Einaudi and others (2003) as being more accurately classed with gold deposits related to reduced granites (e.g., Thompson and Newberry, 2000). Also reduced skarns often occur in clastic sedimentary sequences. The new phase equilibria offered here help explain these observations. Given the common pyrrhotite–pyrite–chalcopyrite sulfide assemblage, their reduced character, and the absence of barite or anhydrite, it is inferred here that a more accurate

name for these systems is reduced intrusion-related copper–gold deposits where the ore-forming fluid may have been derived from metasedimentary wall rocks and convected by heat from the cooling pluton as a sheeted quartz vein system without the local pluton being the dominant source of metals itself, as in porphyry copper deposits. Similarly, the orogenic gold systems may have derived their fluids from metasedimentary wall rocks as metamorphic fluids. Both ore types are labeled here as "OG-IRCG" and are shown in orange (fig. 9). These systems do not fall along the porphyry copper trend but are rather displaced to higher values of H_2S. The carbonate veins lacking sulfate minerals (anhydrite and barite) and methane-rich fluid inclusions and H_2S vapor phase are consistent with this conclusion (Mernagh and Bastrakov, 2013).

CO_2 Release by Limestone or Dolomite Dissolution, Causing Volume Change and Mineralized Breccia Formation

Unlike the normal hydrolysis reactions in PCDs when wall-rock minerals such as plagioclase are altered to sericite or clay minerals *in situ*, when acids dissolve calcite or dolomite, the release of CO_2 causes a very different result: the creation of gas-filled cavities. The potential for deformational mass transfer becomes highly likely (Brimhall and others, 1992). In contrast to water saturation, when porphyritic magmas saturate with water and explode, causing hydrofracturing and transferring the metals from the magma to the hydrothermal fluid, when carbonate minerals dissolve and release a gas phase that is less dense and more compressible than water, the volume change may be negative as void space is created. The potential for brecciation then becomes significant, but with a different mechanism than with typical hydrothermal breccias: collapse rather than explosion. This may explain both the breccia types at Clementine: the mineralized matrix vein breccia system and the earlier barren breccias. The apparent difference is the timing when the fugitive CO_2 gas phase intermingles with the ore-forming hydrothermal fluid. Given the difference in compressibility between CO_2 and water, it is possible that when gas-rich cavities form by carbonate dissolution, they affect the behavior of water in the nearby magma. If the pressure is lowered, then water saturation could be induced in the magma, thus extracting the metals via an escaping hydrothermal fluid. The resultant highly deformed rock mass would be dominated by brecccias to the extent that any hydrothermal breccia formed where water escaped the magma could be obliterated. Similarly, the stockwork of veinlets formed by hydrofracturing may be less well developed or absent. At Clementine, the mineralized matrix vein breccias occurred within throughgoing fractures that formed a vein system that extends for over 1 km. It is possible at depth, however, that the sulfide mineralization is not vein-controlled but instead is more distributed and massive, constituting the matrix between rock fragments.

Hydrothermal Fluid Characteristics

By considering hydrocarbon equilibria along with inorganic mineral assemblages, the phase relations in the CO_2/CH_4-H_2S coordinate system provide a powerful comparative framework for discerning genetic interrelationships expressed within a three-component fluid source mixing model. On one side of the triangle are the chemical evolution trajectories of porphyry copper deposits expressing their origin in granitic magmas, but eventually outrunning their influence as carbon dioxide flooding and sericitization destroys buffer mineral assemblages as oxidation by meteoric water or end-stage magmatic fluids increases the CO_2/CH_4 ratio by 15 orders of magnitude and the oxygen fugacity by 7 orders of magnitude. Sediment-hosted porphyry copper deposits extend this range downward by early high-temperature interactions with surrounding sedimentary wall rock, where diffusion-controlled growth of orbicular actinolite alteration forms and defines the outer edge of advective fluid flow. The CO_2/CH_4 ratio attending orb growth is 0.01 (log = -2), so CH_4 is about 99% and CO_2 is about 1%. Since the orbicular actinolite orb zones are mapped outside the marble front where the temperature was about 400 to 450°C, orbs represent the outer edge of the early high-temperature magmatic hydrothermal phase of PCD growth before incursion of CO_2-rich meteoric water with lower temperatures. Thus, if orbs grew under relatively high temperatures not much below 400°C, it raises questions as to the nature of the pore fluids before mineralization.

Hydrocarbon–Magmatic–Hydrothermal Fluid Mixing

Given the proximity of actinolite orbs and the spectrum of hydrocarbon equilibria derived from basin diagenesis as shown in figure 9, it is possible in some PCD environments for liquid and/or gaseous hydrocarbons generated by maturation of sedimentary organics in source rocks to have migrated into the same domal structure trap/reservoirs where later PCD magmatic/hydrothermal processes occurred. In such cases the apex PCD target environment would have been primed for interaction of hydrocarbons and magmatic–hydrothermal fluids (Zentilli and others, 1997; Ozdemir and Palabiyik, 2019). Comingling of hydrocarbon-rich fluids and hydrothermal fluids could have a spectrum of consequences from oil-filled vacuoles similar to those at the Culver Baer mercury mine in the Coast range, California (Peabody and Einaudi, 1992; Peabody 1993) or degraded bitumen in association with chalcocite, chalcopyrite, and bornite as at El Soldado, Chile (Zentilli and others, 1997), where petroleum occupied the host rock porosity before copper mineralization. At Clementine a central soil anomaly of Hg may be suggestive of such an interplay of hydrocarbons and magmatic–hydrothermal fluids evident in the proximity of the cinnabar–liquid mercury equilibria to the Clementine orb gas composition.

Conclusions

The deep apex sediment-hosted enhanced resource or the DASHER PCD model is presented here, combining PCD mineralization containing Cu, Ag, Sb, As, W, and Ga with earlier sedimentary phosphate with REEs and unconformity-related paleo-karst controlling high-grade Leadville, Colorado-style veins and Cu-Ag mantos since the same Mississippian age unconformity occurs in Montana and Colorado. This DASHER model includes multiple metals on the Critical Minerals list and phosphate. Since the sedimentary sequence at Clementine has 700 m of reactive Madison Limestone and 180 m of carbonaceous Jefferson dolomite at depth, the full range of magma-derived metals may be geochemically expressed in addition to the syngenetic REEs in the Phosphoria Formation. Domestic production of critical and basic minerals from DASHER PCDs could help reduce supply chain vulnerabilities.

However, the occurrence of REEs in the Phosphoria Formation highlights areas of overlapping mineral right laws, as phosphate is leasable while the metals are locatable. The high U content of the Phosphoria provides a means of mapping phosphate using aerial radiometric surveys.

Using chemical thermodynamic principles, a new equilibrium phase diagram proved that distal orbicular actinolite alteration is an integral part of PCD genesis and can be used reliably to help in targeting PCDs. By combining bulk and selective underground mining of the enhanced resource during the mine life cycle, innovative space utilization could minimize the environmental footprint on the surface. Regions where selective mining of phosphate occurs could be used as back-fill zones for development waste rock and flotation and phosphate leach plant gypsum products. Underground mining is primed for innovations in carbon-free electrification and use of autonomous vehicles. Over time, acceptance of the DASHER PCD model and innovations in underground mining might help soften if not transform the current negative attitudes about mining as a purely extractive industry and replace it with understanding of ore deposits as the primary origination point for a sustainable energy future.

Acknowledgments

The 2009 paper by late Harold Helgeson and associates, “A chemical and thermodynamic model of oil generation in hydrocarbon source rocks,” is a milestone in organic geochemistry and provided the chemical thermodynamic data necessary for this study to integrate organic and inorganic species with ore deposit geochemistry. Special gratitude is expressed to Jeff Dick, who patiently guided the first author in the use of his CHNOSZ computing software platform to perform thermodynamic calculations of equilibrium constants for reactions involving organic species and biomolecules included in the Helgeson and others (2009) paper. Kathy Ehrig’s thoughtful discussion significantly improved the fluid mixing interpretation. Marco Einaudi kindly helped to improve the clarity of presentation of the sulfide assemblages of porphyry copper deposits. A review by Alan Boudreau improved the clarity of this paper. Poul Emsbo shared his knowledge of REEs with the author, which is much appreciated. Jay Ague brought to the first author’s attention program SUPCRTBL for thermodynamic modeling, developed by Chen Zhu as a modification of SUPCRT program of the Helgeson Group and also in discussion of CO_2-driven oxidation processes. The author thanks his colleagues in Clementine Exploration for

their abiding interest and support, including Mary Jane Brimhall, Doug Fuerstenau, Ray Morley, Dan Kunz, Ed Rogers, Bruce Marsh, Abel Vanegas, Christ Lewis, and Tim Teague.

References

Ague, J.J., and Brimhall, G.H., 1987, Granites of the batholiths of California: Products of local assimilation and regional-scale crustal contamination: Geology, v. 15, p. 63–66.

Ague, J.J., and Brimhall, G.H.,1988, Regional variations in bulk chemistry, mineralogy, and the compositions of mafic and accessory minerals in the batholiths of California: Geological Society of America Bulletin, v. 100, p. 891–911.

Alpers, C.N., and Brimhall, G.H., 1988, Middle Miocene climatic change in the Atacama Desert, northern Chile: Evidence from supergene mineralization at La Escondida: Geological Society of America Bulletin, v. 100, p. 1640–1656.

Alpers, C.N., and Brimhall, G.H., 1989, Paleohydrologic evolution and geochemical dynamics of cumulative supergene metal enrichment at La Escondida, Atacama Desert, northern Chile: Economic Geology, v. 84, p. 229–255.

Atkinson, W., and Einaudi, M.T., 1978, Skarn formation and mineralization in the contact aureole at Carr Fork, Bingham, Utah: Economic Geology, v. 75, p. 1326–1365.

Ballard, W.W., Bluemle, J.P., and Gerhard, L.C., coordinators, 1983, Northern Rockies/Williston Basin correlation chart, *in* Correlation of stratigraphic units of North America: Tulsa, Oklahoma, American Association of Petroleum Geologists, 1 sheet.

Beaty, D., Landis, G., and Thompson, T., eds., 1990, Carbonate-hosted sulfide deposits of the central Colorado mineral belt: Economic Geology Monograph 7, 417 p.

Brimhall, G.H. Jr., 1973, Mineralogy, texture, and chemistry of early wall rock alteration in the deep underground mines and Continental area, *in* Miller, R.N., ed.,Guidebook for the Butte field meeting of the Society of Economic Geologists: Society of Economic Geologists Guidebook, Anaconda Company, Butte, Montana, p. H1–H5.

Brimhall, G.H., 1977, Early fracture-controlled disseminated mineralization at Butte, Montana: Economic Geology, v. 72, p. 37–59.

Brimhall, G.H, 1979, Lithologic determination of mass transfer mechanisms of multiple stage porphyry copper mineralization at Butte, Montana: Vein formation by hypogene leaching and enrichment of potassium-silicate protore: Economic Geology, v. 74, p. 556–589.

Brimhall, G.H., 1980, Deep hypogene oxidation of porphyry copper potassium-silicate protores: A theoretical evaluation of the copper remobilization hypothesis: Economic Geology, v. 75, p. 384-409.

Brimhall, G.H., 2018, Orbicular alteration at the porphyry copper prospect of southwest Montana: Defining the edges of advective flow in the porphyry copper paradigm: Montana Bureau of Mines and Geology Special Publication 120, p. 71–84.

Brimhall, G.H., and Crerar, D.A., 1987, Ore fluids: Magmatic to supergene, *in* Thermodynamic modeling of geological materials: Minerals, fluids and melts, I. Carmichael and H. Eugster, eds.: Mineralogic Society of America Reviews in Mineralogy, v. 17, ch. 10, p. 235–321.

Brimhall, G.H., and Fanning, M., 2019, Supporting the transition to deep porphyry copper exploration: SHRIMP U/Pb radiometric dating of titanite ($CaTiSiO_5$) in the distal and superjacent orbicular alteration zone of the Clementine prospect, southwest Montana: Montana Bureau of Mines and Geology Special Publication 121, p. 117–132.

Brimhall, G.H., and Ghiorso, M.S., 1983, Origin and ore-forming consequences of the advanced argillic alteration process in hypogene environments by magmatic gas contamination of meteoric fluids: Economic Geology, v. 78, p. 73–90.

Brimhall, G.H., and Marsh, B.D., 2017, Nature of the mineralization and alteration mapped at the Clementine porphyry copper prospect in the northern Pioneer Mountains of southwest Montana: Unpublished Abstract, Montana Bureau of Mines and Geology.

Brimhall, G.H., and Vanegas, A., 2001, Removing science workflow barriers to adoption of digital geological mapping by using the GeoMapper universal program and visual user interface, *in* Soller, D.R., ed., Digital Mapping Techniques ’01—Workshop proceedings: U.S. Geological Survey Open-File Report 01-223, p. 103–114, available at http://pubs.usgs.gov/of/2001/of01-223/brimhall.html [Accessed January 2022].

Brimhall, G.H., Alpers, C.N., and Cunnigham, A.B., 1985a, Analysis of supergene ore-forming processes and ground water solute transport using mass balance principles: Economic Geology, v. 80, p. 1227–1256.

Brimhall, G.H., Agee, C., and Stoffregen, R., 1985b, Hydrothermal conversion of hornblende to biotite: Canadian Mineralogist, v. 23, p. 369–379.

Brimhall, G.H., Chadwick, O.A., Lewis, C.J., Compston, W, Williams, I.S., Danti, K.J., Dietrich, W.E., Power, M.E., Hendricks, D., and Bratt, J., 1992, Deformational mass transport and invasive processes in soil evolution, Science, v. 255, p. 695–702.

Brimhall, G.H., Vanegas, A., and Lerch, D., 2002, GeoMapper Program for paperless field mapping with seamless map production in ESRI ArcMap and GeoLogger for drill-hole data capture: Applications in geology, astronomy, environmental remediation and raised relief models, *in* Soller, D.R., ed., Digital Mapping Techniques’02—Workshop proceedings: U.S. Geological Survey Open-File Report 02-370, p 141–151, available at http://pubs.usgs.gov/of/2002/of02-370/brimhall.html [Accessed January 2022].

Brimhall, G.H., Dilles, J., and Proffett, J., 2006, The role of geological mapping in mineral exploration in wealth creation in the minerals industry: Special Publication 12, Anniversary Publications of the Society of Economic Geologists, p. 221–241.

Brumbaugh, D.S., 1973, Structural analysis of the complexly deformed Big Hole River area, Madison, Beaverhead, and Silver Bow Counties, Montana: Bloomington, Ind., Indiana University, Ph.D. thesis, 96 p.

Candela, P.A., and Piccoli, P. M., 2005, Magmatic processes in the development of porphyry-type ore systems: Economic Geology 100th Anniversary Volume, v. 25–38.

De Voto, 1988, Late Mississippian paleokarst and related mineral deposits, Leadville Formation, central Colorado: Paleokarst, N.Y., Springer-Verlag, p. 278–305.

Dick, Jeffrey M., 2019, CHNOSZ: Thermodynamic calculations and diagrams for geochemistry: Frontiers in Earth Science, available at https://doi.org/10.3389/feart.2019.00180 [Accessed January 2022].

Dickinson, W., 1981, Plate tectonics and the Continental Margin of California, *in* The geotectonic development of California, Rubey Volume: Englewood Cliffs, N.J., Prentice Hall, p. 1–18.

Dilles, J.H., and Einaudi, M.T., 1992, Wall-rock alteration and hydrothermal flow paths about the Ann-Mason porphyry copper-deposit, Nevada—a 6-km vertical reconstruction: Economic Geology, v. 87, p. 1963–2001.

Dott, Robert H. Jr., 1992, Eustasy: The Historical ups and downs of a major geological concept: Geological Society of America Memoir 180, 83–91.

Dott, Robert H. Jr., 2014, Rock Stars: Lawrence L. Sloss and the sequence stratigraphy revolution: GSA Today, March, p. 24–26.

Einaudi, M.T., 1977, Environment of ore deposition at Cerro de Pasco, Peru: Economic Geology, v. 72, p. 893–924.

Einaudi, M.T., Hedenquist, J., and Inan, E., 2003, Sulfidation state of fluids in active and extinct hydrothermal systems, Giggenbach Volume, Simmons, S.F., ed.: Society of Economic Geologists and Geochemical Society Special Publication 10, p. 285–313.

Emsbo, P., McLaughlin, P. I., Breit, G.N., du Bray, E.A., and Koenig, E.A., 2015, Rare earth elements in sedimentary phosphate deposits: Solution to the global REE crisis?: Gondwana Research, v. 27, p. 776–785.

Emsbo, P., McLaughlin, P. I., du Bray, E.A., Anderson, E.A., Vandenbroucke, T.R., and Zielinski, R.A., 2016, Rare Earth elements in sedimentary phosphorite deposits: A global assessment: Reviews in Economic Geology, v. 18, ch. 5, p. 101–113.

Gong, D., Huang, S., Wu, W., Yu, C., Fang, C., and Liu, D., 2014, Characteristics of gas compositions in giant gas fields of China: Energy exploration and Exploitation, v. 32, p. 635–656.

Greenwood, H., 1967, Wollastonite: Stability in H_2O-CO_2 mixtures and occurrence in a contact-metamorphic aureole near Salmo, British Columbia, Canada: American Mineralogist, v. 52, p. 1669–1680.

Guilbert, J.M., and Zeihen, G.L., 1964, The mineralogy of the Butte district, Montana: Montana Bureau of Mines and Geology Open-File Report 268, 38 p.

Gustafson, L.B., and Hunt, J.P., 1975, The porphyry copper deposit at El Salvador, Chile: Economic Geology, v. 70, p. 857–912.

Hein, J., Perkins, R., and McIntyre, 2014, Evolution of thought concerning the origin of the Phosphoria Formation, western U.S. phosphate field, *in* Hein, James R., ed.. Handbook of exploration and environmental geochemistry, v. 8, Hale, M., series ed.: Amsterdam, Elsevier, p. 19-42.

Helgeson, H.C., Delany, J.M., Nesbitt, H.W., and Bird, D.K., 1978, Summary and critique of the thermodynamic properties of rock-forming minerals: American Journal of Science, v. 287-A, p. 1–229.

Helgeson, H.C., Owens, C.E., Knox, A.M., and Laurent, R., 1998, Calculation of the standard molal thermodynamic properties of crystalline, liquid, and gas organic molecules at high temperatures and pressures: Geochimica Cosmochimica Acta, v. 62, p. 985–1081, doi: 10.1016/S0016-7037(97)00219-6

Helgeson, H.C., Laurent, R., McKenzie, W.F., Norton, D.L., and Schmitt, A., 2009, Chemical and thermodynamic model of oil generation in hydrocarbon source rocks: Geochimica Cosmochimica Acta, v. 73, p. 594–695, doi: 10.1016/j.gca.2008.03.004

Hemley, J.J., Montoya, J.W., Marinenko, J.W., and Luce, R.W., 1980, Equilibria in the system Al_2O_3-SiO_2-H_2O and some general implications for alteration/mineralization processes: Economic Geology, v. 75, p. 210–228.

Hildenbrand, T.G., Berger, B.R., Jachens, R.C., and Ludington, S.D., 2000, Regional crustal structures and their relationship to the distribution of ore deposits in the Western United States, based on magnetic and gravity: Economic Geology, v. 95, p. 1583–1603.

Hintze, L.F., 1985, Great Basin correlation chart, *in* Correlation of stratigraphic units of North America: Tulsa, Oklahoma, American Association of Petroleum Geologists.

Hofstra, A., and Cline, J., 2000, Characteristics and models for Carlin-type gold deposits: Society of Economic Reviews, v. 13, p. 163–220.

Holland, H.D., 1959, Some Applications of thermochemical data to problems of ore deposits.stability relations among the oxides, sulfides, sulfates, and carbonates of ore and gangue metals: Economic Geology, v. 54, p. 184-233.

Holland, T., and Powell, R., 2011, An improved and extended internally consistent thermodynamic dataset for phases of petrological interest, involving a new equation of state for solids: Journal Metamorphic Geology, v. 29, p, 333–383.

John, D.A., Ayuso, R.A., Barton, M.D., Blakely, R.J., Bodnar, R.J., Dilles, J.H., Gray, F., Graybeal, F.T., Mars, J.C., McPhee, D.K., Seal, R.R., Taylor, R.D., and Vikre, P.G., 2010, Porphyry copper deposit model, ch. B, *in* Mineral deposit models for resource assessment: U.S. Geological Survey Scientific Investigations Report 2010–5070–B, 169 p.

Johnson, J., Oelkers, E., and and Helgeson, H., 1992, SUPCRT92: A software package for calculating the standard molal thermodynamic properties of minerals, gases, aqueous species, and reactions from 1 to 5000 bar and 0 to 1000°C: Computers and Geoscience, v. 18, no. 7, p. 899–947.

Kalakay, T., John, B., and Lageson, D., 2001, Fault-controlled pluton emplacement in the Sevier fold-and-thrust belt of southwest Montana, USA: Journal of Structural Geology, v. 23, no. 6-7, p. 1151–1165.

Kent, H., Couch, E., and Knepp, R., 1988, Southern and central Rockies, *in* Correlation of stratigraphic units of North America: Tulsa, Oklahoma, American Association of Petroleum Geologists.

Khashgerel, B., Kavalieris, I., and Hayashi**,** K., 2008, Mineralogy, textures, and whole-rock geochemistry of advanced argillic alteration: Hugo Dummett porphyry Cu–Au deposit, Oyu Tolgoi mineral district, Mongolia: Mineralia Deposita, v. 43, p. 913–932.

Lageson, D., and Schmidt, J., 1994, The Sevier orogenic belt of the western United States: Recent advances in understanding its structural and sedimentologic framework: Mesozoic Systems of the Rocky Mountain Region, USA, AAPG Data Pages, p. 27–64.

Lanari, P., and Duesterhoeft, E., 2019, Modeling metamorphic rocks using equilibrium thermodynamics and internally consistent databases: Past achievements, problems and perspectives: Journal of Petrology, v. 60., no. 1, p. 19–56.

Lowell, J.D., and Guilbert, J., 1970, Lateral and vertical alteration-mineralization zoning in porphyry ore deposits: Economic Geology, v. 65, p. 373–408.

Meinert, L., 1982, Skarn, manto, and breccia pipe formation in sedimentary rocks of the Cananea mining district, Sonora, Mexico: Economic Geology, v. 77, p. 919–949.

Mernagh, T.P., and Bastrakov, E.N., 2013, An evaluation of hydrogen sulfide in orogenic gold fluids and the uncertainties associated with vapor-rich inclusions: Geofluids, v. 13, p. 494–505.

Meyer, C., and Hemley, J.J., 1967, Wall rock alteration, *in* Barnes, H.L., ed., Geochemistry of hydrothermal ore deposits: N.Y., Holt, Rinehart, and Winston, p. 166–232.

Meyer, C., Shea, E., Goddard, C., and staff, 1968, Ore deposits at Butte, Montana, *in* Ridge, J.D.,ed., Ore deposits of the United States 1933–1967, The Graton-Sales Volume: N.Y., American Institute of Mining, Metallurgical, and Petroleum Engineers, v. 2, p. 1363–1416.

National Research Council, 2013, Underground engineering for sustainable urban development: Washington, DC, The National Academies Press, 221 p., doi: https://doi.org/10.17226/14670.

Nemcok, M., and Henk, A., 2006, Oil reservoirs in foreland basins charged by thrust belt source rocks: Insights from numerical stress modelling and geometric balancing in the West Carpathians: Geological Society London Special Publications v. 253, no. 1, p. 415–428.

Pearson, R., Trautwein, C., Ruppel, E., Hanna, W., Rowan, L., Loen, J., and Berger, B., 1992, Mineral resource assessment of the Dillon 1° x 2° quadrangle, Idaho and Montana: U.S. Geological Survey Circular 1077, 14 p.

Ozdemir, A., and Palabiyik, Y., 2019, Significance of relationships between hydrocarbons and metallic ore deposits in oil and gas exploration: Part II. Copper deposits: Ankara, Turkey, Conference Proceedings.

Peabody, C., 1993, The association of cinnabar and bitumen in mercury deposits of the California Coast Ranges, *in* Parnell, J., and others, eds., Bitumens in ore deposits: Berlin, Springer-Verlag, p. 178–209.

Peabody, C., and Einaudi, M., 1992, Origin of petroleum and mercury in the Culver Baer cinnabar deposit, Mayacmas District, California: Economic Geology, v. 87, p. 1078–1103.

Roberts, S.A., 1973, Pervasive early alteration in the Butte district, Montana, *in* Miller, R.N., ed., Guidebook for the Butte field meeting of the Society of Economic Geologists: Society of Economic Geologists Guidebook, Anaconda Company, Butte, Montana, p. HH1–HH8.

Roberts, S.A., 1975, Early hydrothermal alteration and mineralization in the Butte district, Montana: Harvard University, Ph.D. dissertation, 157 p.

Rowins, S.M., 2000, Reduced porphyry copper-gold deposits: A new variation on an old theme: Geology, v. 28, no. 6, p. 491–494.

Runyon, S., Nickerson, P., Seedorff, E., Barton, M., and Mazdab, F., 2018, Sodic-calcic family of alteration in porphyry systems of Arizona and adjacent New Mexico: Economic Geology, v. 114, p. 745–770.

Ruppel, E.T., and Lopez, D., 1984, The thrust belt in southwest Montana and east-central Idaho: U.S. Geological Survey Professional Paper 1278, 41 p.

Ruppel, E.T., O'Neill, J.M., and Lopez, D.A., 1993, Geologic map of the Dillon 1° x 2° quadrangle, Idaho and Montana: U.S. Geological Survey Miscellaneous Investigation Series 1803-H.

Sando, W.J., 1988, Madison Limestone (Mississippian) Paleokarst: A geologic synthesis: Paleokarst, N.Y., Springer-Verlag, p. 256–277.

Schmidt, C., Smedes, H., and O'Neill, M., 1990, Syncompressional emplacement of the Boulder and Tobacco Root Batholiths (Montana-USA) by pull-apart along Old Fault Zones: Geological Journal, v. 25, no. 304, p. 305–318.

Seedorff, E., Dilles, J., Proffett, J., Einaudi, M., Zurcher, L., Stavast, W., Johnson, D., and Barton, M., 2005, Porphyry deposits: Characteristics and origin of hypogene features: Economic Geology 100th Anniversary Volume, p. 251–298.

Sheppard, M.F., and Taylor, H.P., Jr., 1974, Hydrogen and oxygen isotope evidence for the origins of water in the Boulder batholith and Butte ore deposits, Montana: Economic Geology, v. 69, p. 926–946.

Sillitoe, R., 2010, Porphyry copper systems: Economic Geology, v. 105, no. 1, p. 3–41.

Sloss, L., 1963, Sequences in the cratonic interior of North America: Gcological Society of America Bulletin, v. 74, p. 93–114.

Sloss, L., and Laird, W.M., 1947, Devonian system in central and northwestern Montana: Bulletin of the American Association of Petroleum Geologists, v. 31, no. 8, p. 1404–1430.

Sloss, L., and Moritz, C.A., 1951, Paleozoic stratigraphy of southwestern Montana: Bulletin of the Society of Petroleum Geologists, v. 35, no. 10, p. 2135–2169.

Taylor, H.P. Jr., 1974, The application of oxygen and hydrogen isotope studies to problems of 1035 hydrothermal alteration and ore deposition: Economic Geology, v. 69, p. 843–883.

Thompson, J.F.H., and Newberry, R.J., 2000, Gold deposits related to reduced granitic intrusions: Reviews in Economic Geology, v. 13, p. 377–400.

Tomkins, A., and Grundy, C., 2009, Upper temperature limits of orogenic gold deposit formation: Constraints from the granulite-hosted Griffin's Find Deposit, Yilgarn craton: Economic Geology, v. 104, pp. 669–685.

Underground Engineering for Sustainable Urban Development, 2013, The National Academies Press, 221 p.

Vail, P.R., and Mitchum, R.M., 1977a, Seismic stratigraphy and global changes of sea level, Part 1: Overview, *in* Payton, C.E., ed., Seismic stratigraphy—Applications to hydrocarbon exploration: AAPG Memoir 26, p. 51–52.

Vail, P.R., Mitchum, R.M., Todd, R.G., Widmier, J.M., Thompsom, S., Sangree, J.B., Bubb, J.N., and Hailelid, W.G., 1977b, Seismic stratigraphy and global changes in sea level, *in* Payton, C.E., ed., Seismic stratigraphy—Applications to hydrocarbon exploration: AAPG Memoir 26, p. 49–212.

Windman, T., and Shock, W., 2008, A web-based interactive version of SUPCRT92: Computers & Geosciences, v. 90, part A, May 2016, p. 97–111.

Wood, B.J., 1987, Thermodynamics of multicomponent systems containing several solid solutions, *in* Carmichael, I.S.E. and Eugster, H.P., eds., Thermodynamic modeling of geological materials: Minerals, fluids and melts: Mineralogical Society of America, Reviews in Mineralogy, v. 17, p. 71–95.

Woodhead, J., and Mathieu, L., 2021, Harnessing the power of artificial intelligence and machine learning in mineral exploration—Opportunities and cautionary notes: SEG Discovery, October, p. 19–31.

Worden, R.H., Griffiths, J., Wooldridge, L.J., Utley, J.E.P., Lawan, A.Y., Muhammed, D.D., Simon, N., and Armitage, P.J., 2020, Chlorite in sandstones: Earth-Science Reviews, v. 204, doi: 10.1016/j.earsci-rev.2020.103105.

Zentilli, M., Munizaga, F., Graves, M., Boric, R., Wilson, N., Mukhopadhyay, P., and Snowdon, L., 1997, Hydrocarbon involvement in the genesis of ore deposits: An example in cretaceous stratabound (manto-type) copper deposits of central Chile: International Geology Review, v. 39, p. 1–21.

Zen, E-An, 1988, Bedrock geology of the Vipond Park quadrangle: U.S. Geological Survey Bulletin 1625, 49 p.

Zimmer, K., Zhang, Y., Peng, L., Yanyan, C., Guanru, Z., Mehmet, D., and Zhu, C., 2016, SUPCRTBL: A revised and extended thermodynamic dataset and software package of SUPCRT92: Computers & Geosciences, v. 90, part A, p. 97–111.

The Montana Tunnels open pit mine. Photo by Peter Larson.